Inorganic Chemistry
Cite This: Inorg. Chem. XXXX, XXX, XXX−XXX
Article
pubs.acs.org/IC

Cyclometalated Ruthenium(II) Complexes Derived from α-Oligothiophenes as Highly Selective Cytotoxic or Photocytotoxic Agents

Goutam Ghosh,[†] Katsuya L. Colón,[‡] Anderson Fuller,[†] Tariq Sainuddin,[†] Evan Bradner,[‡] Julia McCain,[†] Susan M. A. Monro,[†] Huimin Yin,[†] Marc W. Hetu,[†] Colin G. Cameron,*[,‡] and Sherri A. McFarland*[,†,‡]

[†]Department of Chemistry, Acadia University, Wolfville, Nova Scotia B4P 2R6, Canada

[‡]Department of Chemistry and Biochemistry, The University of North Carolina at Greensboro, Greensboro, North Carolina 27402, United States

Supporting Information

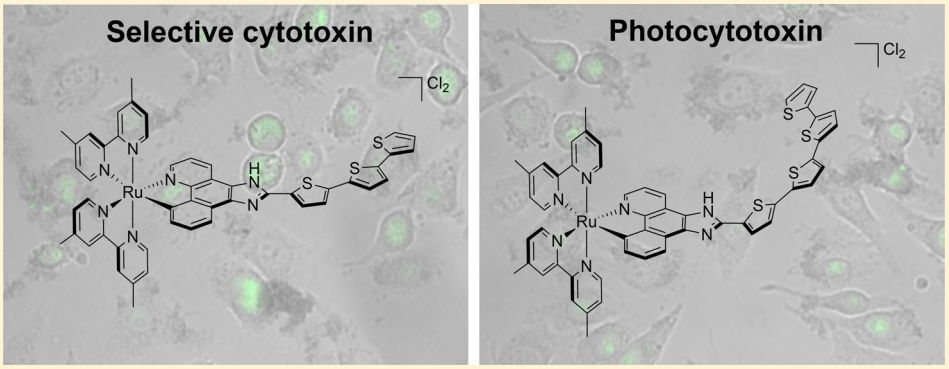

ABSTRACT: The photophysical and photobiological properties of a new class of cyclometalated ruthenium(II) compounds incorporating π-extended benzo[*h*]imidazo[4,5-*f*]quinoline (IBQ) cyclometalating ligands (C^N) bearing thienyl rings (*n* = 1−4, compounds **1**−**4**) were investigated. Their octanol−water partition coefficients (log $P_{o/w}$) were positive and increased with *n*. Their absorption and emission energies were red-shifted substantially compared to the analogous Ru(II) diimine (N^N) complexes. They displayed C^N-based intraligand (IL) fluorescence and triplet excited-state absorption that shifted to longer wavelengths with increasing *n* and N^N-based metal-to-ligand charge transfer (MLCT) phosphorescence that was independent of *n*. Their photoluminescence lifetimes (τ_{em}) ranged from 4−10 ns for ^{1}IL states and 12−18 ns for ^{3}MLCT states. Transient absorption lifetimes (τ_{TA}) were 5−8 μs with 355 nm excitation, ascribed to ^{3}IL states that became inaccessible for **1**−**3** with 532 nm excitation (**1**−**3**, τ_{TA} = 16−17 ns); the ^{3}IL of **4** only was accessible by lower energy excitation, τ_{TA} = 3.8 μs. Complex **4** was nontoxic (EC_{50} > 300 μM) to SK-MEL-28 melanoma cells and CCD1064-Sk normal skin fibroblasts in the dark, while **3** was selectively cytotoxic to melanoma (EC_{50}= 5.1 μM) only. Compounds **1** and **2** were selective for melanoma cells in the dark, with submicromolar potencies (EC_{50} = 350−500 nM) and selectivity factors (SFs) around 50. The photocytotoxicities of compounds **1**−**4** toward melanoma cells were similar, but only compounds **3** and **4** displayed significant phototherapeutic indices (PIs; **3**, 43; **4**, >1100). The larger cytotoxicities for compounds **1** and **2** were attributed to increased cellular uptake and nuclear accumulation, and possibly related to the DNA-aggregating properties of all four compounds as demonstrated by cell-free gel mobility-shift assays. Together, these results demonstrate a new class of thiophene-containing Ru(II) cyclometalated compounds that contain both highly selective chemotherapeutic agents and extremely potent photocytotoxic agents.

1. INTRODUCTION

Ru(II) polypyridyl complexes (RPCs) have been studied extensively over the years, notably as photosensitizers for a variety of light-based applications and in more fundamental studies of energy- and electron-transfer. The continued interest in RPCs stems, in part, from their strong absorption of visible light that produces relatively long-lived triplet metal-to-ligand charge transfer (MLCT) excited states ($\tau \approx 1$ μs) as well as their attractive redox properties.[1−4] More recently, RPCs are being explored as light-responsive agents for photobiological applications such as photodynamic therapy (PDT) and photochemotherapy (PCT),[5−7] and as photocaging units for precise delivery of enzyme inhibitors.[8,9] Our RPC TLD1433 just successfully completed a Phase 1b clinical trial for treating bladder cancer with PDT (ClinicalTrials.gov Identifier: NCT03053635), which is the first example of a Ru(II)-based photosensitizer that has advanced to human studies.

Received: March 14, 2018

DOI: 10.1021/acs.inorgchem.8b00689
Inorg. Chem. XXXX, XXX, XXX−XXX

Chart 1. Molecular Structures of Ru(II) C^N Complexes 1−4

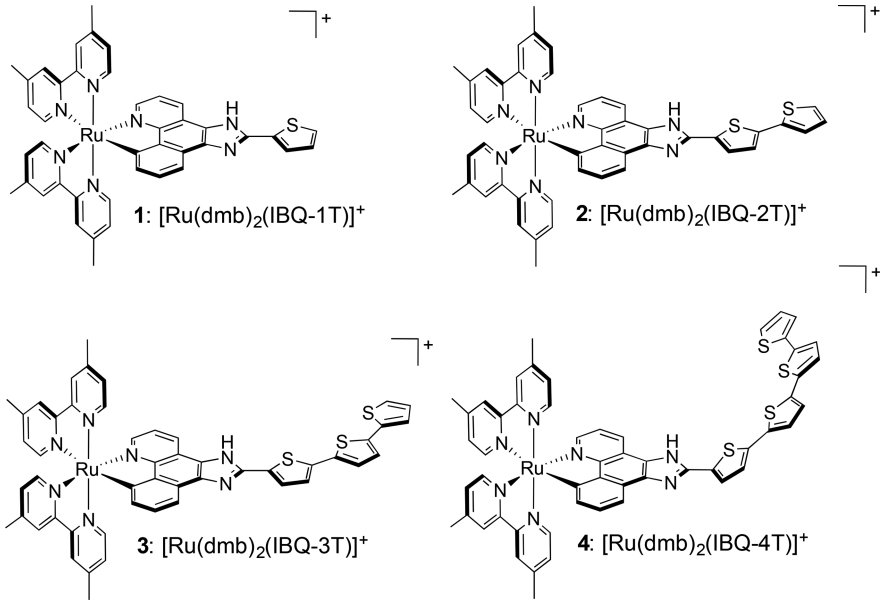

Briefly, PDT/PCT collectively refer to phototherapy approaches that utilize an inherently nontoxic, light-responsive compound that can be activated with photons to destroy cancer cells with spatiotemporal selectivity. PDT refers to photosensitization mechanisms that involve reactive oxygen species (notably singlet oxygen, $^1O_2$), whereas PCT is defined by oxygen-independent processes. Herein, we use the term PDT tentatively since the mechanism has not been definitively established (and could include both PDT and PCT since they are not necessarily mutually exclusive). Recent 2017 reviews by Gunnlaugsson and co-workers and Turro and co-workers. contain notable highlights with regard to the use of light-responsive RPCs in photobiology and photomedicine.[10,11]

While RPCs and Ru(II) diimine (N^N) complexes in general have been widely studied, the related cyclometalated (C^N) complexes are understudied by comparison. Fewer than 20 $[Ru(LL)2(C^N)]^+$ complexes appeared in the Cambridge Structural Database (CSD) as of 2015, and these are based on C^N = $phpy^-$ (deprotonated phenylpyridine) or derivatives of $phpy^-$.[12,13] Similarly, modest metal-based oxidation potentials, short excited-state lifetimes, and weak photoluminescence, in part related to excited state dynamics dictated by the energy gap law,[14] have limited the utility of Ru(II) C^N complexes for many photonic applications despite their potential as panchromatic light-harvesting dyes.[15] These characteristics also limit the utility of such organometallic complexes for PDT, and their low-energy ^{3}MLCT states also prohibit access to triplet metal-centered (^{3}MC) states that permit photoinduced ligand substitution reactions, one of the established PCT mechanisms.[16] In addition, a variety of Ru(II) C^N systems have been shown to be too cytotoxic to be useful for any type of phototherapy that requires a nontoxic, prodrug photosensitizer.[16−18]

Ru(II) C^N complexes of the type $[Ru(bpy)(phpy^-)(LL)]Cl$ (where bpy = 2,2′-bipyridine, LL = 1,10-phenanthroline (phen), dipyrido[3,2-*f*:2′,3′-*h*]quinoxaline (dpq), dipyrido[3,2-*a*:2′,3′-*c*]phenazine (dppz), or benzo[*i*]dipyrido[3,2-*a*;2′,3′-*c*]phenazine (dppn)) are cytotoxic compounds without light activation and have been categorized as potential chemotherapeutics rather than phototherapy agents.[18,19] We previously demonstrated that this is also the case for some $[Ru(bpy)_2(C^N)]Cl$ complexes, where the C^N ligand is benzo[*h*]quinoline (bhq^-), 4,9,12-triazadibenzo[*a*,*c*]-naphthalene ($pbpq^-$), or 4,9,14-triazadibenzo[*a*,*c*]anthracene ($pbpz^-$).[17] These anionic ligands systematically extend π-conjugation with an increase in the number of fused aromatic rings and are the C^N analogs of the well-studied phen, dpq, and dppz N^N ligands. Interestingly, the Ru(II) C^N complex derived from the more π-expansive 4,9,16-triazadibenzo[*a*,*c*]-naphthacene ($pbpn^-$) exhibited no cytotoxicity and acted as a potent in vitro light-responsive agent, with a phototherapeutic index larger than 1400 and nanomolar photocytotoxicity (EC_{50} ≈ 200 nM).[17] The abrupt reduction in cytotoxicity on going from pbpz to pbpn as the C^N ligand demonstrated that not all Ru(II) C^N complexes are inherently cytotoxic.

The fact that Ru(II) C^N complexes tend to be more photochemically stable than their analogous Ru(II) N^N complexes and that their absorption profiles are significantly red-shifted (by at least 100 nm) are two reasons why there is ongoing interest in developing these cyclometalated systems for phototherapy applications. The desire to capitalize on these attractive properties and to understand the unexpected change in cytotoxicity with the pbpn C^N ligand prompted us to investigate whether π-extended C^N ligands of a critical degree of conjugation could be a general phenomenon for reducing the cytotoxicity of Ru(II) C^N systems. On the basis of this premise, four new compounds were synthesized and characterized, where an α-oligothiophene unit serves as a convenient handle for systematically extending π-conjugation. Complexes **1**−**4** (Chart 1) are based on the analogous N^N series[20] that contains our lead photosensitizer TLD1433. Compound **3** is the C^N analog of TLD1433. In the present Ru(II) cyclometalated series, the C^N ligand is IBQ-*n*T, where the IBQ framework is substituted with thienyl rings to successively extend π-conjugation from n = 1 to 4. We hypothesized that there would be a critical number n for reducing cytotoxicity in order to afford meaningful in vitro phototherapeutic effects.

DOI: 10.1021/acs.inorgchem.8b00689
Inorg. Chem. XXXX, XXX, XXX−XXX

2. EXPERIMENTAL PROCEDURES

2.1. General. Unless noted otherwise, all reagents and solvents were obtained from commercial sources and used without further purification. $[Ru(4,4'\text{-dmb})_2Cl_2]\cdot 2H_2O$,[21] benzo[*h*]quinoline-5,6-dione,[22] and 5-bromo-5″-formyl-2,2′:5′,2″-terthiophene[23] were prepared according to established procedures.

2.2. Instrumentation. Microwave reactions were performed in a CEM Discover microwave reactor. ^{1}H NMR spectra were collected using a Bruker AVANCE 500 (Dalhousie University Nuclear Magnetic Resonance Research Resource) or 300 (Acadia Centre for Microstructural Analysis) MHz spectrometer, and high- and low-resolution ESI mass spectra were obtained using a Bruker microTOF focus mass spectrometer (Dalhousie University Mass Spectrometry Laboratory). HPLC analyses were performed using an Agilent 1100 series instrument (ChemStation Rev. A 10.02 software) using a Hypersil GOLD C18 reverse phase column with an A-B gradient (98% → 5% A; A = 0.1% formic acid in H_2O, B = 0.1% formic acid in MeOH). Reported retention times are correct to within ±0.1 min.

2.3. Synthesis. The aldehydes 1T-CHO, 2T-CHO, and 3T-CHO were obtained commercially. 4T-CHO was prepared as described below from 5-bromo-5″-formyl-2,2′:5′,2″-terthiophene, which was synthesized according to a literature procedure.[23] The IBQ-*n*T ligands and their corresponding Ru(II) C^N complexes have not been reported and have been characterized by TLC, ^{1}H NMR, mass spectrometry, and HPLC. The Ru(II) C^N complexes were isolated as their PF_6^- salts for characterization and converted to their Cl^- salts for biological studies.

[2,2′:5′,2″:5″,2‴-Tetrathiophene]-5-carbaldehyde (4T-CHO). To an oven-dried 50 mL Schlenk flask, purged with argon, were added dry DMF (20 mL), 2-(tributylstannyl)thiophene (1.164 g, 3.08 mmol), 5-bromo-5″-formyl-2,2′:5′,2″-terthiophene (1.013 g, 2.85 mmol), and tetrakis(triphenylphosphine)palladium(0) (64 mg, 0.086 mmol) to obtain a bright orange solution. The reaction mixture was heated at 80 °C overnight, resulting in a dark red solution. The mixture was concentrated under reduced pressure for an hour and dried in a vacuum oven at 70 °C. The crude product was purified through recrystallization, using hot acetone, to obtain the desired product as a dark orange solid (0.598 g, 59%). R_f = 0.8 (1% MeOH in DCM). ^{1}H NMR (300 MHz, chloroform-*d*, ppm): δ 9.86 (s, 1H; CHO), 7.67 (d, J = 4.0 Hz, 1H; g), 7.28 (d, J = 3.9 Hz, 1H; h), 7.26−7.23 (m, 3H; i,j,k), 7.20 (dd, J = 3.7, 1.1 Hz, 1H; o), 7.14−7.09 (m, 2H; l,m), 7.04 (dd, J = 5.1, 3.6 Hz, 1H; n). HPLC retention time: 33.19 min.

2-(2-Thiophene)-1H-benzo[h]imidazo[4,5-f]quinoline (IBQ-1T). Benzo[*h*]quinoline-5,6-dione (209 mg, 1.2 mmol), thiophene-2-carbaldehyde (93 μL, 1.0 mmol), and ammonium acetate (2.5 g, 32 mmol) were added to a 100 mL round-bottom flask with glacial acetic acid (30 mL). The orange mixture was heated at reflux (118 °C) for 48 h, which resulted in a dark red solution. The solution was cooled to ambient temperature, then neutralized with NH_4OH. The precipitate was vacuum filtered with a fine sintered-glass frit and washed with cold deionized water (30 mL) and diethyl ether (200 mL) to obtain the desired product as a brown solid (85 mg, 28%). R_f = 0.69 (1% MeOH in DCM). ^{1}H NMR (500 MHz, DMSO-d_6, ppm): δ 9.26 (d, J = 8.2 Hz, 1H), 8.97 (d, J = 3.7 Hz, 1H), 8.83 (d, J = 7.9 Hz, 1H), 8.51 (d, J = 7.9 Hz, 1H), 7.94 (d, J = 3.6 Hz, 1H), 7.84 (dd, J = 7.5 Hz, 1H), 7.80−7.74 (m, 2H), 7.71 (dd, J = 7.6 Hz, 1H), 7.30 (dd, J = 4.3 Hz, 1H). HPLC retention time: 28.31 min.

2-(2,2′-Bithiophene)-1H-benzo[h]imidazo[4,5-f]quinoline (IBQ-2T). Benzo[*h*]quinoline-5,6-dione (231 mg, 1.1 mmol), 2,2′-bithiophene-5-carbaldehyde (194 mg, 1.0 mmol), and ammonium acetate (2.5 g, 32 mmol) were added to a 100 mL round-bottom flask with glacial acetic acid (30 mL). The orange mixture was heated at reflux (118 °C) for 41 h, which resulted in a dark red solution. The solution was cooled to ambient temperature, then neutralized with NH_4OH. The precipitate was vacuum filtered with a fine sintered-glass frit and washed with cold deionized water (50 mL), cold ethanol (50 mL), and diethyl ether (400 mL) to obtain the desired product as a brown solid (207 mg, 54%). R_f = 0.81 (1% MeOH in DCM). ^{1}H NMR (500 MHz, DMSO-d_6, ppm): δ 9.26 (d, J = 8.2 Hz, 1H), 8.98 (dd, J = 4.3, 1.7 Hz, 1H), 8.82 (dd, J = 8.1, 1.7 Hz, 1H), 8.49 (d, J = 7.9 Hz, 1H), 7.89−7.83 (m, 2H), 7.77 (dd, J = 8.1, 4.4 Hz, 1H), 7.72 (t, J = 8.3, 6.8, 1.2 Hz, 1H), 7.61 (dd, J = 5.1, 1.1 Hz, 1H), 7.49 (dd, J = 3.6, 1.1 Hz, 1H), 7.47 (d, J = 3.8 Hz, 1H), 7.18 (dd, J = 5.1, 3.6 Hz, 1H). HPLC retention time: 32.15 min.

2-(2,2′:5′,2″-Terthiophene)-1H-benzo[h]imidazo[4,5-f]quinoline (IBQ-3T). Benzo[*h*]quinoline-5,6-dione (251 mg, 1.2 mmol), [2,2′:5′,2″-terthiophene]-5-carbaldehyde (276 mg, 1.0 mmol), and ammonium acetate (2.5 g, 32 mmol) were added to a 100 mL round-bottom flask with glacial acetic acid (30 mL). The orange mixture was heated at reflux (118 °C) for 23 h, which resulted in a dark red solution. The solution was cooled to ambient temperature, then neutralized with NH_4OH. The precipitate was vacuum filtered with a fine sintered-glass frit and washed with cold deionized water (30 mL) and diethyl ether (300 mL) to obtain the desired product as a brown solid (254 mg, 55%). R_f = 0.84 (1% MeOH in DCM). ^{1}H NMR (500 MHz, DMSO-d_6, ppm): δ 9.26 (d, J = 8.2 Hz, 1H), 8.98 (dd, J = 4.2, 1.9 Hz, 1H), 8.82 (d, J = 7.9 Hz, 1H), 8.49 (d, J = 7.8 Hz, 1H), 7.90−7.83 (m, 2H), 7.78 (dd, J = 8.0, 4.3 Hz, 1H), 7.72 (dd, J = 7.6 Hz, 1H), 7.58 (d, J = 4.9 Hz, 1H), 7.50 (d, J = 3.9 Hz, 1H), 7.46 (d, J = 3.8 Hz, 1H), 7.41 (d, J = 3.5 Hz, 1H), 7.35 (d, J = 3.8 Hz, 1H), 7.15 (dd, J = 5.1, 3.6 Hz, 1H). HPLC retention time: 34.37 min.

2-(2,2′:5′,2″:5″,2‴-Tetrathiophene)-1H-benzo[h]imidazo[4,5-f]-quinoline (IBQ-4T). Benzo[*h*]quinoline-5,6-dione (88 mg, 0.42 mmol), [2,2′:5′,2″:5″,2‴-tetrathiophene]-5-carbaldehyde (126 mg, 0.35 mmol), and ammonium acetate (863 mg, 11 mmol) were added to a 100 mL round-bottom flask with glacial acetic acid (20 mL). The orange mixture was heated at reflux (118 °C) for 46 h. The mixture was cooled to ambient temperature, then neutralized with NH_4OH. The precipitate was vacuum filtered with a fine sintered-glass frit and washed with cold deionized water (50 mL) and diethyl ether (250 mL) to obtain the desired product as a brown solid (38 mg, 20%). R_f = 0.86 (1% MeOH in DCM). ^{1}H NMR (300 MHz, DMSO-d_6, ppm): δ 9.26 (d, J = 8.2 Hz, 1H), 8.98 (dd, J = 4.3, 1.6 Hz, 1H), 8.83 (dd, 1H), 8.50 (d, J = 8.1 Hz, 1H), 7.91 (d, J = 4.0 Hz, 1H), 7.85 (d, J = 7.2 Hz, 1H), 7.80−7.73 (m, 1H), 7.71 (d, J = 7.7 Hz, 1H), 7.62−7.56 (m, 2H), 7.48 (d, J = 3.8 Hz, 1H), 7.41−7.37 (m, 3H), 7.33 (d, J = 3.8 Hz, 1H), 7.13 (dd, J = 4.4 Hz, 1H). HPLC retention time: 33.18 min.

[Ru(dmb)$_2$(IBQ-1T)]PF$_6$ (1). $Ru(dmb)_2Cl_2\cdot 2H_2O$ (124 mg, 0.21 mmol) and IBQ-1T (50 mg, 0.16 mmol) were added to a microwave vessel with triethylamine (1 mL) and ethylene glycol (3 mL). The mixture was microwaved at 120 °C for 1 h. The purple mixture was poured into approximately 25 mL of stirring, saturated KPF_6 solution. The resulting precipitate was vacuum filtered with a fine sintered-glass frit and washed with deionized water (100 mL) and diethyl ether (200 mL). The crude product was purified by silica gel column chromatography with 1% MeOH in DCM to obtain the desired product as a purple solid (50 mg, 25%). R_f = 0.42 (2% MeOH in DCM). ^{1}H NMR (500 MHz, acetonitrile-d_3, ppm): δ 11.63 (s, 1H; −NH), 8.64 (d, J = 7.9 Hz, 1H; c), 8.36 (s, 1H; 3A), 8.24 (s, 1H, 3B), 8.23 (s, 1H, 3C), 8.17 (s, 1H; 3D), 7.86−7.82 (m, 3H; f, a, 6A), 7.76 (d, J = 5.9 Hz, 1H; 6C), 7.72−7.69 (m, 2H; 6B, g), 7.57 (d, J = 4.0 Hz, 1H; i), 7.46 (d, J = 5.9 Hz, 1H; 6D), 7.35 (dd, J = 8.0, 5.3 Hz, 1H; b), 7.32 (dd, J = 5.4, 2.3 Hz, 1H; h), 7.28 (d, J = 7.5 Hz, 1H; 5A), 7.25 (dd, J = 5.1, 3.7 Hz, 1H; e), 7.14 (dd, J = 5.8, 1.0 Hz, 1H; 5B), 6.87 (d, J = 5.9 Hz, 2H; 5C, 5D), 6.73 (d, J = 7.1 Hz, 1H; d), 2.56 (s, 3H; 4A-Me), 2.53 (s, 3H; 4B-Me), 2.52 (s, 3H; 4C-Me), 2.51 (s, 3H; 4D-Me). MS (ESI+) m/z: 770.2 $[M\text{-}PF_6]^+$. HRMS (ESI+) m/z for $C_{42}H_{34}N_7RuS$ calcd: 770.164. Found: 770.1631. HPLC retention time: 27.53 min.

[Ru(dmb)$_2$(IBQ-2T)]PF$_6$ (2). $Ru(dmb)_2Cl_2\cdot 2H_2O$ (195 mg, 0.33 mmol) and IBQ-2T (100 mg, 0.26 mmol) were added to a microwave vessel with triethylamine (1 mL) and ethylene glycol (3 mL). The mixture was microwaved at 120 °C for 1 h. The purple mixture was poured into approximately 25 mL of stirring, saturated KPF_6 solution. The resulting precipitate was vacuum filtered with a fine sintered-glass frit and washed with deionized (100 mL) water and diethyl ether (200 mL). The crude product was purified by silica gel column chromatography with 0.80% MeOH in DCM to obtain the desired

DOI: 10.1021/acs.inorgchem.8b00689
Inorg. Chem. XXXX, XXX, XXX−XXX

product as a purple solid (60 mg, 18%). R_f = 0.43 (2% MeOH in DCM). ^{1}H NMR (500 MHz, cetonitrile-d_3, ppm): δ 11.64 (s, 1H; −NH), 8.61 (s, 1H; c), 8.36 (s, 1H; 3A), 8.25 (s, 1H, 3B), 8.23 (s, 1H, 3C), 8.17 (s, 1H; 3D), 7.87−7.81 (m, 2H; f, 6A), 7.76 (d, J = 6.0 Hz, 1H; 6C), 7.73 (d, J = 3.9 Hz, 1H; a), 7.70 (d, J = 5.8 Hz, 2H; 6B, g), 7.48−7.43 (m, 2H; 6D, k), 7.41 (dd, J = 3.7, 1.1 Hz, 1H; i), 7.36−7.33 (m, 2H; b, h), 7.32 (dd, J = 5.7, 1.4 Hz, 1H; 5A), 7.27 (dd, J = 7.5 Hz, 1H; e), 7.14 (dd, J = 5.1, 3.3 Hz, 2H; 5B, j), 6.89−6.87 (m, 2H; 5C, 5D), 6.73 (d, J = 7.1 Hz, 1H; d), 2.56 (s, 3H; 4A-Me), 2.51 (s, 3H; 4B-Me), 2.40 (s, 3H; 4C−Me), 2.38 (s, 3H; 4D-Me). MS (ESI+) m/z: 852.2 $[M\text{-}PF_6]^+$. HRMS (ESI+) m/z for $C_{46}H_{36}N_7RuS_2$ calcd: 852.1517. Found: 852.1507. HPLC retention time: 29.09 min.

*[Ru(dmb)$_2$(IBQ-3T)]PF$_6$ (**3**).* $Ru(dmb)_2Cl_2{\cdot}2H_2O$ (80 mg, 0.13 mmol) and IBQ-3T (50 mg, 0.11 mmol) were added to a microwave vessel with triethylamine (1 mL) and ethylene glycol (3 mL). The mixture was microwaved at 120 °C for 1 h. The purple mixture was poured into approximately 25 mL of stirring, saturated KPF_6 solution. The resulting precipitate was vacuum filtered with a fine sintered-glass frit and washed with deionized water (100 mL) and diethyl ether (200 mL). The crude product was purified by silica gel column chromatography with 0.75% MeOH in DCM to obtain the desired product as a purple solid (35 mg, 25%). R_f = 0.43 (2% MeOH in DCM). ^{1}H NMR (500 MHz, acetonitrile-d_3, ppm): δ 11.68 (s, 1H; −NH), 8.63 (d, J = 8.0 Hz, 1H; c), 8.36 (s, 1H; 3A), 8.25 (s, 1H, 3B), 8.23 (s, 1H, 3C), 8.17 (s, 1H; 3D), 7.86 (d, J = 5.1 Hz, 1H; f), 7.83 (d, J = 5.6 Hz, 1H; 6A), 7.77 (d, J = 6.0 Hz, 1H; 6C), 7.73 (d, J = 4.0 Hz, 1H; a), 7.71−7.68 (m, 2H; 6B, g), 7.47 (d, J = 6.0 Hz, 1H; 6D), 7.42 (d, J = 5.2 Hz, 1H; m), 7.37−7.35 (m, 1H; b), 7.34−7.30 (m, 4H; h, i, j, k), 7.28 (d, J = 8.1 Hz, 1H; 5A), 7.25 (d, J = 3.9 Hz, 1H; e), 7.15−7.10 (m, 2H; 5B, l), 6.89 (d, J = 4.9 Hz, 2H; 5C, 5D), 6.73 (d, J = 7.2 Hz, 1H; d), 2.56 (s, 3H; 4A-Me), 2.51 (s, 3H; 4B-Me), 2.40 (s, 3H; 4C-Me), 2.38 (s, 3H; 4D-Me). MS (ESI+) m/z: 934.2 $[M\text{-}PF_6]^+$. HRMS (ESI+) m/z for $C_{50}H_{38}N_7RuS_3$ calcd: 934.1394. Found: 934.1405. HPLC retention time: 30.54 min.

*[Ru(dmb)$_2$(IBQ-4T)]PF$_6$ (**4**).* $Ru(dmb)_2Cl_2{\cdot}2H_2O$ (135 mg, 0.23 mmol) and IBQ-4T (100 mg, 0.18 mmol) were added to a microwave vessel with triethylamine (1 mL) and ethylene glycol (3 mL). The mixture was microwaved at 120 °C for 1 h. The purple mixture was poured into approximately 25 mL of stirring, saturated KPF_6 solution. The resulting precipitate was vacuum filtered with a fine sintered-glass frit and washed with deionized water (100 mL) and diethyl ether (200 mL). The crude product was purified by silica gel column chromatography with 1% MeOH in DCM to obtain the desired product as a purple solid (25 mg, 9%). R_f = 0.43 (2% MeOH in DCM). ^{1}H NMR (500 MHz, acetonitrile-d_3, ppm): δ 11.71 (s, 1H; -NH), 8.64 (d, J = 7.9 Hz, 1H; c), 8.35 (s, 1H; 3A), 8.24 (s, 1H, 3B), 8.22 (s, 1H, 3C), 8.16 (s, 1H; 3D), 7.86 (d, J = 5.2 Hz, 1H; f), 7.83 (d, J = 5.6 Hz, 1H; 6A), 7.78 (d, J = 6.0 Hz, 1H; 6C), 7.72−7.67 (m, 3H; a, g, 6B), 7.47 (d, J = 6.0 Hz, 1H; 6D), 7.39 (d, J = 5.0 Hz, 1H; m), 7.35 (dd, J = 6.7 Hz, 1H; b), 7.32−7.25 (m, 5H; o, h, 5A, e, i), 7.19−7.17 (m, 2H; j, k), 7.14−7.12 (m, 2H; 5B, l), 7.10 (dd, J = 4.4 Hz, 1H; n), 6.87 (d, J = 5.9 Hz, 2H; 5C, 5D), 6.74 (d, J = 7.3 Hz, 1H; d), 2.55 (s, 3H; 4A-Me), 2.50 (s, 3H; 4B-Me), 2.39 (s, 3H; 4C−Me), 2.37 (s, 3H; 4D-Me). MS (ESI+) m/z: 1016.1 $[M\text{-}PF_6]^+$. HRMS (ESI+) m/z for $C_{54}H_{40}N_7RuS_4$ calcd: 1016.1271. Found: 1016.1267. HPLC retention time: 31.61 min.

2.4. Lipophilicity. The lipophilicities of the C^N complexes were determined using a modified "shake flask" method. A saturated solution of 1-octanol with water was prepared by mixing 16 mL of 1-octanol (99.9%) with 4 mL of deionized water (Milli-Q), and a saturated solution of water with 1-octanol was prepared by mixing 16 mL of deionized water (Milli-Q) with 4 mL of 1-octanol (99.9%). The saturated solutions were shaken for 24 h at ambient temperature using a New Brunswick Classic C25KC Incubator Shaker set at 230 rpm before further use. A 50 μM solution of each C^N complex was prepared in 500 μL of saturated 1-octanol, and an equal volume of saturated water was added to give a total volume of 1 mL. The mixtures were shaken 200 times, centrifuged at 11 000 rpm for 2 min using a BioRad Model 16K Microcentrifuge, and then separated. The concentrations of the C^N complexes in both the octanol and water layers were calculated from absorption measurements using a microplate reader (SpectraMax M2^e).

2.5. Spectroscopy. Photophysical characterization was carried out on dilute solutions (5−20 μM) of the PF_6^- salts of the metal complexes in spectroscopic grade MeCN unless otherwise noted. The molar extinction coefficient (ε) at local maxima in the UV−vis spectra were determined from the slope of absorption versus concentration for five concentrations (20 μM and four serial dilutions of 25%) and measured in duplicate. Quantum yields for emission (Φ_{em}) and singlet oxygen (Φ_Δ) were measured relative to $[Ru(bpy)_3](PF_6)_2$ according to eq 1, where I, A, and η are the integrated emission intensity, the absorbance at the excitation wavelength, and the refractive index of the solvent, respectively, and the subscript s denotes the standard. Reference quantum yields used for $[Ru(bpy)_3](PF_6)_2$ are Φ_{em} = 0.012 at 298 K in aerated MeCN,[24] Φ_{em} = 0.095 at 298 K in deaerated MeCN,[25] Φ_{em} = 0.38 at 77 K in frozen 4:1 v/v EtOH/MeOH,[1] and Φ_Δ = 0.56 in aerated MeCN.[26]

$$\Phi = \Phi_s\left(\frac{I}{A}\right)\left(\frac{A_s}{I_s}\right)\left(\frac{\eta^2}{\eta_s^2}\right) \quad (1)$$

Solutions were degassed by argon sparging in a long-stemmed cuvette (Luzchem QSC10S) for emission experiments, or by five freeze−pump−thaw cycles for transient absorption using custom-fabricated Schlenk-style cuvettes. Samples for 77 K measurements were prepared in a 4:1 EtOH/MeOH solution in a 5 mm i.d. NMR tube, frozen in liquid nitrogen in a quartz-tipped coldfinger Dewar (Wilmad Labglass).

UV−vis absorption spectra were recorded on a Jasco V-730 spectrometer. Steady-state luminescence spectra were measured on a PTI Quantamaster equipped with a K170B PMT for measuring ultraviolet to visible emission and a Hamamatsu R5509-42 NIR PMT for measuring NIR emission (<1400 nm) and quantifying $^1O_2$ emission (centered around 1276 nm). Emission and excitation spectra were corrected for the wavelength dependence of lamp output and detector response.

Transient absorption (TA) spectra and lifetimes were measured on an Edinburgh Instruments LP-980 spectrometer equipped with a PMT-LP detector and a Continuum Minilite Nd:YAG laser using a 355 or 532 nm pump wavelength (7−9 mJ pulse^{-1}). This instrumentation was also used in its fluorescence mode to measure emission lifetimes.

2.6. Cellular Assays. *2.6.1. Metal Complex Solutions.* The Cl^- salts of the Ru(II) cyclometalated complexes were prepared as stock solutions for cellular assays at 5 mM in water containing 10% DMSO and stored at −20 °C prior to use. Working dilutions were made by diluting the aqueous stock with Dulbecco's phosphate buffered saline (DPBS) at pH 7.4. DPBS is a balanced salt solution of 1.47 mM potassium phosphate monobasic, 8.10 mM sodium phosphate dibasic, 2.68 mM potassium chloride, and 0.137 M sodium chloride (no Ca^{2+} or Mg^{2+}). DMSO in the assay wells was under 0.1% at the highest metal complex concentration.

2.6.2. Cell Culture. SK-MEL-28 Human Melanoma Cells. Adherent SK-MEL-28 malignant melanoma cells (ATCC HTB-72) were cultured in Eagle's Minimum Essential Medium (EMEM; Mediatech Media MT-10-009-CV) supplemented with 10% FBS (PAA Laboratories, A15−701) and were incubated at 37 °C under 5% CO_2 and passaged two to three times per week according to standard aseptic procedures. SK-MEL-28 cells were started at 200 000 cells mL^{-1} in 75 cm^2 tissue culture flasks and were subcultured when growth reached 550 000 cells mL^{-1} by removing the old culture medium and rinsing the cell layer once with Dulbecco's phosphate-buffered saline (DPBS 1X, Mediatech, 21-031 CV) followed by dissociation of cell monolayer with 1X Trypsin−EDTA solution (0.25% w/v Trypsin/0.53 mM EDTA, ATCC 30−2101). Complete growth medium was added to the cell suspension to allow appropriate aliquots of cells to be transferred to new cell vessels. Complete growth medium was prepared in 250 mL portions as needed by combining EMEM (225 mL) and FBS (25 mL, prealiquoted, and heat

DOI: 10.1021/acs.inorgchem.8b00689
Inorg. Chem. XXXX, XXX, XXX−XXX

inactivated) in a 250 mL Millipore vacuum stericup (0.22 μm) and filtering.

CCD-1064Sk Human Skin Fibroblast Cells. Adherent CCD-1064Sk normal skin fibroblasts (ATCC CRL-2076) were cultured in Iscove's Modified Dulbecco's Medium (IMDM; HyClone, SH30228.01) supplemented with 10% FBS (PAA Laboratories, A15-701), incubated at 37 °C under 5% CO_2 and were passaged two to three times per week according to standard aseptic procedures. CCD-1064Sk cells were started at 200 000 cells mL^{-1} in 75 cm^2 tissue culture flasks and were subcultured when growth reached 550 000 cells mL^{-1} by removing the old culture medium and rinsing the cell monolayer once with Dulbecco's phosphate-buffered saline (DPBS 1X, Mediatech, 21-031-CV), followed by dissociation of the cell monolayer with trypsin–EDTA solution (0.25% w/v Trypsin/0.53 mM EDTA, ATCC 30-2101). Complete growth medium was added to the cell suspension to allow appropriate aliquots of cells to be transferred to new cell vessels. Complete growth medium was prepared in 250 mL portions as needed by combining IMDM (225 mL) and FBS (25 mL, prealiquoted, and heat inactivated) in a 250 mL Millipore vacuum stericup (0.22 μm) and filtering.

2.6.3. Cytotoxicity and Photocytotoxicity. Cell viability experiments were performed in triplicate in 96-well TC-treated microtiter plates (Corning Costar, Acton, MA), where outer wells along the periphery contained 200 μL of DPBS (2.68 mM potassium chloride, 1.47 mM potassium phosphate monobasic, 0.137 M sodium chloride, and 8.10 mM sodium phosphate dibasic) to minimize evaporation from sample wells. Cells growing in log phase (SK-MEL-28 and CCD-1064Sk cells: ~550 000–600 000 cells mL^{-1}) with at least 93% viability were transferred in 50 μL aliquots to inner wells containing warm culture medium (25 μL) and placed in a 37 °C, 5% CO_2 water-jacketed incubator (Thermo Electron Corp., FormaSeries II, model 3110, HEPA Class 100) for 3 h to equilibrate (and allow for efficient cell attachment in the case of adherent cells).

Ru-based compounds were serially diluted with DPBS and prewarmed at 37 °C before 25 μL aliquots of the appropriate dilutions were added to cells. PS-treated microplates were incubated at 37 °C under 5% CO_2 for 16 h drug-to-light intervals. Control microplates not receiving a light treatment were kept in the dark in an incubator (but removed from the incubator and kept in the dark for the same amount of time that the light-treated samples were outside of the incubator), and light-treated microplates were irradiated under one of the following conditions: visible light (400–700 nm, 34.7 mW cm^{-2}) using a 190 W BenQ MS 510 overhead projector or red light (625 nm, 27.8 mW cm^{-2}) from an LED array (PhotoDynamic Inc., Halifax, NS). Irradiation times using these two light sources were approximately 48 and 60 min, respectively, to yield total light doses of 100 J cm^{-2}.

Both untreated and light-treated microplates were incubated for another 48 h before 10 μL aliquots of prewarmed Alamar Blue reagent (Life Technologies DAL 1025) were added to all sample wells and subsequently incubated for another 15–16 h. Cell viability was determined on the basis of the ability of the Alamar Blue redox indicator to be metabolically converted to a fluorescent dye by only live cells. Fluorescence was quantified with a Cytofluor 4000 fluorescence microplate reader with the excitation filter set at 530 ± 25 nm and emission filter set at 620 ± 40 nm.

The effective concentrations required to reduce cell viability by 50% (EC_{50}) were calculated from sigmoidal fits of the dose–response curves for dark (cytotoxicity) and light (photocytotoxicity) treatments using Graph Pad Prism 6.0 according to eq 2 (below), where y_i and y_f are the initial and final fluorescence signal intensities. For cells growing in log phase and of the same passage number, EC_{50} values are generally reproducible to within ±25% in the submicromolar regime, ±10% below 10 μM, and ±5% above 10 μM. Phototherapeutic indices (PIs), a measure of the therapeutic window, were calculated from the ratio of dark to light EC_{50} values obtained from the dose–response curves. Selectivity factors (SFs), a measure of the selective cytotoxicity of the compounds toward cancer cells over normal cells, were calculated from the ratio of the dark EC_{50} values for SKMEL28 melanoma cells and CCD-1064Sk human skin fibroblasts.

$$y = y_i + \frac{y_i - y_f}{1 + 10^{(\log EC_{50} - x)\times(\text{Hillscope})}} \quad (2)$$

2.7. DNA Mobility-Shift Assays. The DNA interactions of cyclometalated Ru compounds were assessed according to a general plasmid DNA gel mobility shift assay with 20 μL total sample volumes in 0.5 mL microfuge tubes. Transformed pUC19 plasmid (2.2 μL, 95% form I) was added to 10 μL of 10 mM Tris-HCl buffer supplemented with 100 mM NaCl (pH 7.5). Serial dilutions of the Ru compounds were prepared in doubly distilled water (ddH2O) and added in 5-μL aliquots to the appropriate tubes to yield final Ru concentrations ranging from 5 to 40 μM. Then, ddH_2O was added to bring the final assay volumes to 20 μL (2.8 μL). Control samples with no metal complex received 7.8 μL of water. Sample tubes were kept at 37 °C in the dark or irradiated. Light treatments employed visible light (14 J cm^{-2}, 7.8 mW cm^{-2}) delivered from a Luzchem LZC-4X photoreactor over the course of 30 min. A softer light dose, relative to that used in the cellular assays, was required to see the topological changes to DNA before the DNA became too distorted to be imaged with the intercalating dye. After treatment, all samples (dark and light) were quenched by the addition of 4 μL of gel loading buffer (0.025% bromophenol blue, 40% glycerol). Samples (11.8 μL) were loaded onto 1% agarose gels cast with 1× TAE (40 mM Tris-acetate, 1 mM EDTA, pH 8.2) and electrophoresed in 1 × TAE at 8 V cm^{-1} for 30 min. The gels were stained with 5 μg mL^{-1} ethidium bromide (in 1 × TAE) for 30 min, then destained in dI water for 30 min. The bands were visualized using the Gel Doc-It Imaging system (UVP) with Vision Works software and further processed with the GNU Image Manipulation Program (GIMP).

2.8. Confocal Microscopy. Sterile glass-bottom Petri dishes (MatTek) were coated with 200 μL of poly-L-lysine (Ted Pella) in a laminar flow hood under standard aseptic conditions. After a 1 h incubation period at 37 °C, 5% CO_2 in a water-jacketed incubator (Thermo Electron Corp., Forma Series II, Model 3110, HEPA class 100), the dishes were washed three times with sterile Dulbecco's phosphate buffered saline (DPBS, Mediatech, 21-031-CV) containing 2.68 mM potassium chloride, 1.47 mM potassium phosphate monobasic, 0.137 M sodium chloride, and 8.10 mM sodium phosphate dibasic, at pH 7.4, and were left to dry uncovered at room temperature for approximately 15 min. SK-MEL-28 malignant melanoma cells (ATCC HTB-72) and CCD-1064Sk normal skin fibroblasts (ATCC CRL-2076) were then transferred in aliquots of 500 μL (approximately 100 000 cells) to the poly-L-lysine-coated glass bottom Petri dishes and were allowed to adhere for 2 h in a 37 °C, 5% CO_2 water-jacketed incubator. A metal compound (500 μL of a 50 μM solution in sterile PBS prewarmed to 37 °C) was added to sample dishes (destined to receive either a dark or light treatment), which were returned to the incubator for 15 min prior to further treatment; control dishes that did not contain the metal compound were also prepared. Light-treated samples were irradiated with visible light for 24 min from a 190 W BenQ MS 510 overhead projector (400–700 nm, power density = 34.7 mW cm^{-2}, total light dose ≈ 50 J cm^{-2}). Dark samples were covered with foil and placed in a drawer for the same amount of time. Cells were then imaged at 15 min post-treatment using a Carl Zeiss LSM 510 laser scanning confocal microscope with a 40× oil objective lens. Excitation was delivered at 458/488 nm from an argon–krypton laser, and signals were acquired through a 505-nm long-pass filter. Pinhole diameters for all the treatments were 100 μm. The images were collected and analyzed using the Zeiss LSM Image Browser Version 4.2.0.121 software (Carl Zeiss Inc.).

3. RESULTS AND DISCUSSION

3.1. Synthesis and Characterization. A growing number of functionalized C^N ligands are being considered for dye-sensitized solar cells (DSSCs)[27,28] given the important discovery that $phpy^-$ substituted with electron-withdrawing groups can produce Ru(II) complexes with conversion efficiencies as large as the isothiocyanate-based champion dyes.[29] Nevertheless, the functionalization of $phpy^-$ has

DOI: 10.1021/acs.inorgchem.8b00689
Inorg. Chem. XXXX, XXX, XXX–XXX

typically only included substitution with electron-withdrawing atoms, groups, or rings, and the use of other C^N ligands such as bhq$^-$ is even more limited. We have recently made a focused effort to fill this gap and expand the number and types of C^N ligands to include those with π-extended frameworks.[17,30] While our focus has been on the use of π-expansive C^N ligands for Ru(II)- and Ir(III)-based photodrugs, the systems may prove useful for other light-based applications. In this study, our emphasis is on π-extended C^N ligands for Ru(II) that contain α-oligothiothiophenes.

Cyclometalated complexes **1**−**4** were synthesized according to adapted literature procedures.[17,31] Briefly, [Ru(4,4′-dmb)$_2$Cl$_2$]·2H$_2$O and the corresponding ligands (IBQ-*n*T, *n* = 1, 2, 3, 4) were combined in 1:3 NEt$_3$/ethylene glycol and subjected to microwave irradiation at 120 °C for 1 h to afford complexes **1**−**4** as their PF$_6^-$ salts in 9−25% yield after silica gel purification. Structural and photophysical characterization was carried out on the PF$_6^-$ salts in MeCN to aid in comparison to published studies on Ru(II) N^N and C^N complexes commonly reported for this salt form and in this solvent. The PF$_6^-$ salts were converted in quantitative yield to their water-soluble Cl$^-$ salts for biological studies using ion-exchange chromatography. The Cl$^-$ salt is the most common form reported in biological testing of Ru(II) complexes. We were unable to obtain crystals for X-ray crystallographic studies so the Ru(II) complex structures were confirmed by a very detailed analysis using 1D and 2D ^{1}H NMR methods.

The IBQ-*n*T ligands used to make the final Ru(II) C^N complexes were prepared via the Radziszewski reaction, whereby benzo[*h*]quinoline-5,6-dione was refluxed with the corresponding thienylcarboxaldehyde and ammonium acetate in glacial acetic acid for 23−48 h.[32] The desired ligands were obtained in low to moderate yield (20−55%) and used without further purification despite minor contamination with unreacted aldehyde in some cases. The starting material benzo[*h*]quinoline-5,6-dione was synthesized in almost quantitative yield by the oxidation of bhq with iodopentoxide in glacial acetic acid.[33] The thienylcarboxaldehydes were obtained commercially except for 4T-CHO, which was synthesized in 59% yield after recrystallization via a Stille coupling from 2-(tributylstannyl)thiophene and 5-bromo-5″-formyl-2,2′:5′,2″-terthiophene in DMF using tetrakis(triphenylphosphine)-palladium(0) as the catalyst. To our knowledge, the ligands IBQ-1T, IBQ-2T, IBQ-3T, and IBQ-4T and their corresponding Ru(II) C^N complexes have not been reported. The target ligands and complexes (as well as 4T-CHO) were characterized by 1D ^{1}H and 2D ^{1}H−^{1}H COSY NMR (Figures S1−S9), mass spectrometry, and HPLC.

We previously characterized bhq and benzo[*h*]quinoline-5,6-dione by ^{1}H−^{1}H COSY NMR spectroscopy, correcting a previous assignment in the 1D ^{1}H NMR spectrum of bhq.[17] The hydrogen NMR assignments for these simple precursors and the more complex Ru(II) C^N systems derived from deprotonated bhq, pbpq, pbpz, and pbpn (and the free ligands) previously reported by us aided in the assignment of the hydrogen NMR spectra for the present series. Chemical shifts for hydrogen atoms associated with the free ligands dissolved in DMSO-d_6 were assigned based on their coupling constants and 2D ^{1}H−^{1}H correlation with neighboring protons.[17] The imidazo NH hydrogen was not discernible in the ^{1}H NMR spectra collected for the IBQ-*n*T ligands in DMSO-d_6. The relative chemical shifts and splitting patterns for hydrogens *a*−*f* and *x* of the bhq unit (Chart 2, Figures S2−S5) were similar for

Chart 2. Structures of C^N Ligands with Position Labels for ^{1}H NMR Assignments[a]

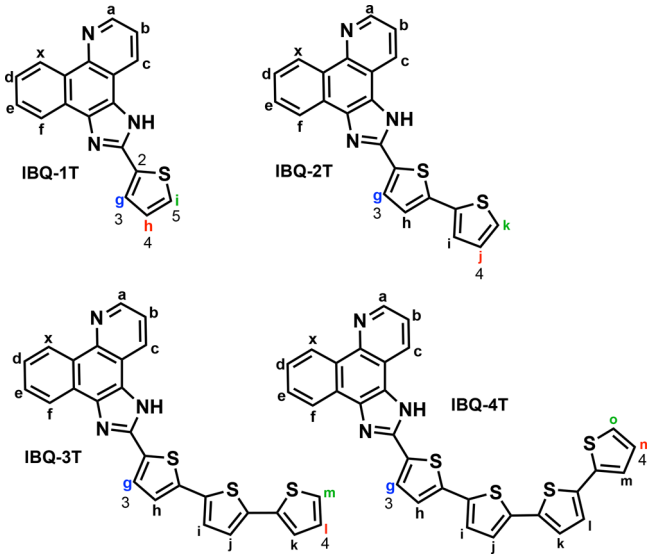

[a]Color scheme for thienyl hydrogens: blue (most deshielded thienyl hydrogen), green (second most deshielded thienyl hydrogen), and red (most shielded thienyl hydrogen).

all four IBQ-*n*T ligands: *x* > *a* > *c* > *f* > *e* > *b* > *d*. The hydrogens influenced by nearby imidazo nitrogen atoms (*x*, *a*, *c*, and *f*) exhibited the largest downfield shifts (8.4−9.4 ppm). Hydrogen *x* was the most deshielded position (>9 ppm) owing to its strong interaction with the quinoline nitrogen, followed by hydrogens *a* and *c* (8.8−9.0 ppm), which are ortho and para to the quinoline nitrogen, respectively. Hydrogen *f*, while not influenced by the quinoline nitrogen, was affected by the imidazo nitrogen and appeared near 8.5 ppm. By comparison, hydrogens *e*, *b*, and *d* were more shielded, appearing between 7.6 and 8.0 ppm.

The thienyl chain(s) of the free ligands exhibited two diagnostic hydrogen signals in the ^{1}H NMR spectra. The hydrogen at position 4 of the distal thiophene ring of each ligand (Chart 2, red positions) was the most shielded aromatic hydrogen of the thienyl rings and gave rise to a signal near 7.1−7.3 ppm that was well separated from the other aromatic peaks. Hydrogen *g* of the proximal thienyl ring (Chart 2, blue positions) was the most deshielded of the thienyl hydrogens, which gave rise to peaks near 7.9 ppm for all of the ligands, followed by the hydrogen at position 5 of the distal thiophene rings (Chart 2, green positions). The rest of the thienyl hydrogen signals for ligands containing two or more thiophenes fell between 7.3 and 7.7 ppm.

Due to the asymmetry of the C^N ligands, the two symmetric 4,4′-dmb ligands of each Ru(II) complex possess 12 unique aromatic hydrogens across pyridyl rings A−D (Chart 3, Figures S6−S9). The four different C^N ligands of this study yield a total of 21, 23, 25, and 27 nonequivalent aromatic hydrogens for complexes **1**, **2**, **3**, and **4**, respectively. Close scrutiny of the similarities and differences in the 1D and 2D ^{1}H NMR spectra for the ligands and complexes of the present series (with systematic extension by one thiophene unit) alongside our previous characterization of [Ru(bpy)$_2$(C^N)](PF$_6$)$_2$ complexes (C^N = bhq$^-$, pbpq$^-$, pbpz$^-$, or pbpn$^-$) made it possible to assign complex spectra with overlapping multiplets.

DOI: 10.1021/acs.inorgchem.8b00689
Inorg. Chem. XXXX, XXX, XXX−XXX

Chart 3. Structures of Ru(II) C^N Complexes with Position Labels for ^{1}H NMR Assignments

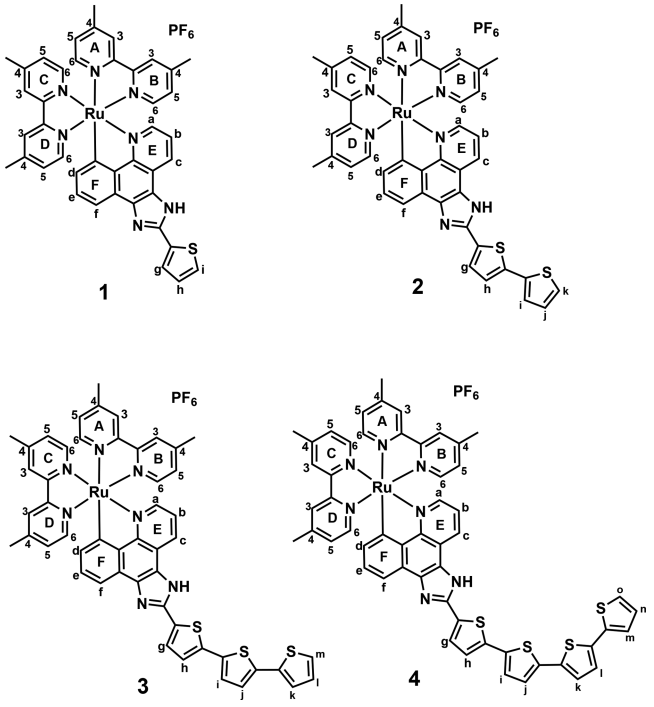

The basis for our interpretation rests on X-ray crystallographic evidence that shortened Ru−C bond distances lead to elongated Ru−N bonds *trans* to the Ru−C coordination axis[34] and that there is a similar but attenuated effect on the Ru−N bonds *cis* to this axis.[35] These distortions in the Ru(II) C^N complexes bring ring F and its hydrogens closer to the metal center while rings A, B, and E and their respective hydrogens are pushed farther away relative to the analogous Ru(II) N^N systems (Chart 3). The impact of this distortion was greatest for hydrogens *d* and *c* of the Ru(II)-coordinated C^N ligand (Figure 1).

In all the complexes investigated, hydrogen *d* next to the shorted Ru−C bond of ring F was the most shielded aromatic position (doublet at 6.73−6.74 ppm), and hydrogen *c* para to the Ru−N bond of ring E and in close proximity to the imidazo N was the most deshielded aromatic C−H position (doublet at 8.61−8.64 ppm). The highest frequency signal for all of the Ru(II) C^N complexes dissolved in MeCN-d_3 was due to the imidazo NH hydrogen, which was not apparent for the C^N ligands dissolved in DMSO-d_6, and ranged from 11.63 to 11.71 ppm, with the broadened signal shifting slightly downfield with increasing number of thiophenes on going from **1** to **4**. The rest of the Ru(II) coordinated C^N ligand hydrogens were assigned based on their couplings in the ^{1}H−^{1}H COSY spectra for the complexes (and their respective ligands) and by comparing these correlations between the ligands and complexes of the same series (Figures S2−S9).

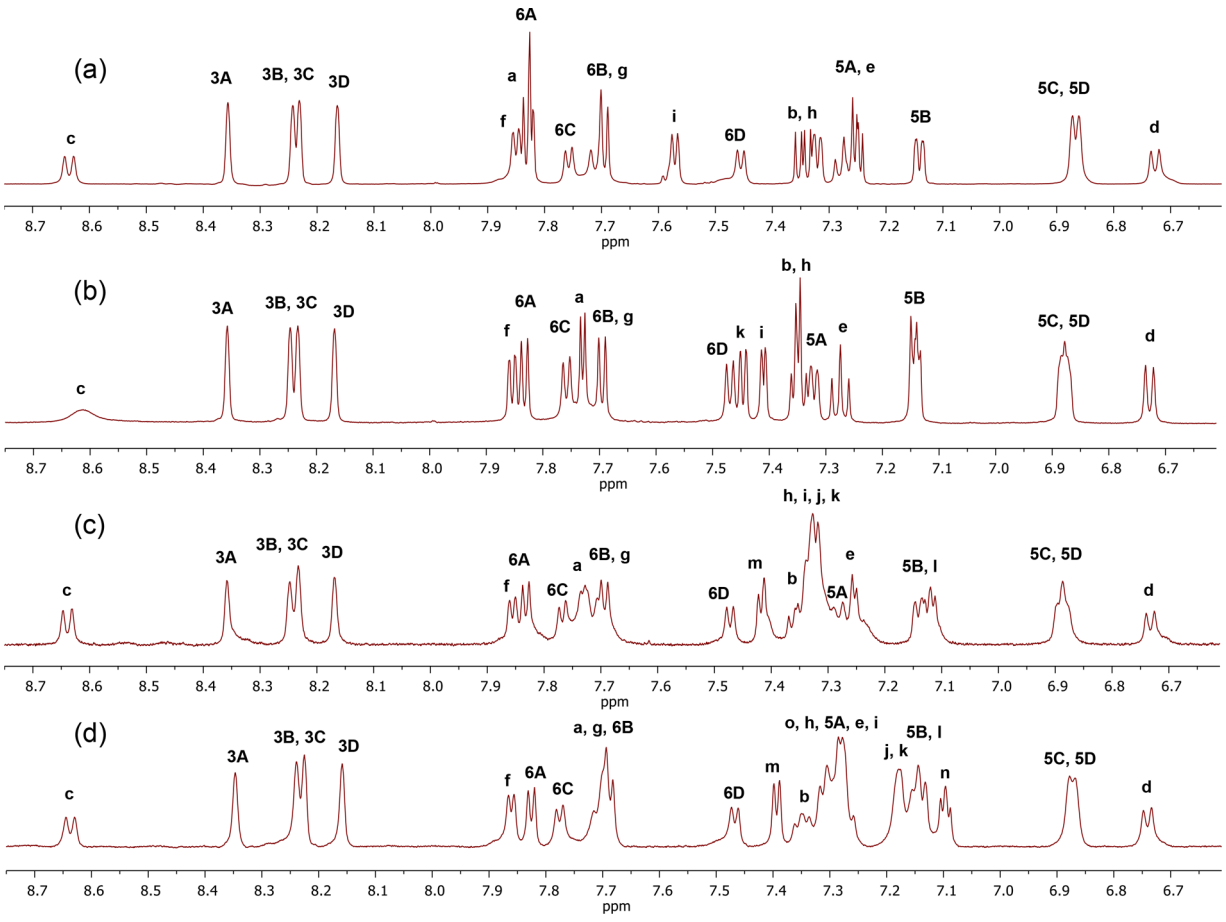

Figure 1. ^{1}H NMR spectra collected for Ru(II) C^N complexes **1** (a), **2** (b), **3** (c), and **4** (d) as their PF_6^- salts in d_3-MeCN.

DOI: 10.1021/acs.inorgchem.8b00689
Inorg. Chem. XXXX, XXX, XXX−XXX

The resonant frequencies for all 12 nonequivalent 4,4′-dmb hydrogens of **1**−**4** (Chart 3) were assigned based on general trends for *cis*-$[Ru(bpy)_2LL]^{2+}$ complexes (whereby H3 > H4 ∼ H6 > H5),[35,36] the bond distances reported by Sasaki et al. for cyclometalated Ru(II) complexes of $phpy^-$,[34] $^1H-^1H$ correlations, and coupling constants. Lack of H4 hydrogens in complexes **1**−**4** due to substitution by methyl groups at these positions rendered the H3 hydrogens particularly diagnostic, appearing as singlets (8.1−8.4 ppm) downfield of the rest of the H6 and H5 hydrogens. The chemical shifts of the 4,4′-dmb hydrogen signals generally increased in the order A > B > C > D except for H6 hydrogens where C > D. The hydrogens of ring A were the most deshielded of the 4,4′-dmb hydrogens due to the longer Ru−N bond distance reported for ring A, where the hydrogens on ring D were the most shielded due to their proximity to ring E of the C^N ligand. Within any one 4,4′-dmb ring, the chemical shifts followed the order H3 > H6 > H5 with no exceptions.

The methyl hydrogen signals of the 4,4′-dmb ligands appeared as four distinct singlets between 2.36−2.58 ppm for complexes **2**−**4** and between 2.50−2.57 ppm for complex **1**. The relative chemical shifts of these hydrogen signals followed the same order for all of the complexes (4A-Me > 4B-Me > 4C-Me > 4D-Me), with the methyl groups of ring D being the most shielded. The thiophene chains had a notable impact on the methyl substituent hydrogens of both rings C and D. The presence of two or more thiophenes in the chain, as in complexes **2**−**4**, shifted the signals for these hydrogens upfield by over 0.1 ppm relative to **1** (Figures S6−S9). In addition, the signals for the 4C-Me and 4D-Me groups appeared closer together in **2**−**4**. While the 4D-Me hydrogens are shielded the most owing to their proximity to the Ru−C bond of ring F, incorporation of two or more thienyl groups into the C^N ligand appears to affect the chemical environment of the 4C-Me hydrogens slightly more. Interestingly, increasing the number of thienyl groups beyond two had very little effect on the methyl groups of rings C and D. In other words, the critical change occurs between n = 1 and 2. The methyl groups of ring A were unaffected by changes to the number of thienyl groups, possibly due to the increased Ru−N bond distance arising from the *trans* effect discussed earlier, and the 4B-Me group hydrogens were only slightly affected.

3.2. Lipophilicity. The lipophilicities of the Ru(II) C^N compounds were assessed by their octanol−water partition coefficients (log $P_{o/w}$), which have previously been used to gauge cell membrane permeability. A positive log $P_{o/w}$ indicates preferential solubility of a compound in the octanol layer, while a negative log $P_{o/w}$ indicates a preference for water. Cyclometalated Ru(II) systems have been shown to be more lipophilic than their RPC counterparts and thus yield more positive log $P_{o/w}$ values.[19] This trend held for compounds **1**−**4**, which yielded positive log $P_{o/w}$ values, and the parent diimine $[Ru(bpy)_3]Cl_2$, which gave a negative log $P_{o/w}$. There was a positive correlation between the number of thiophenes in the IBQ-*n*T ligand and the lipophilicities of the overall complexes (Figure 2), with compound **4** being the most lipophilic and **1** being the least. On the basis of the premise that cellular uptake increases with lipophilicity[19,37,38] and that uptake impacts cytotoxicity, compound **4** might be expected to be the most cytotoxic compound of the series. However, **4** was the least cytotoxic (vide infra) in the series, highlighting the importance of factors other than lipophilicity in determining cytotoxicity.

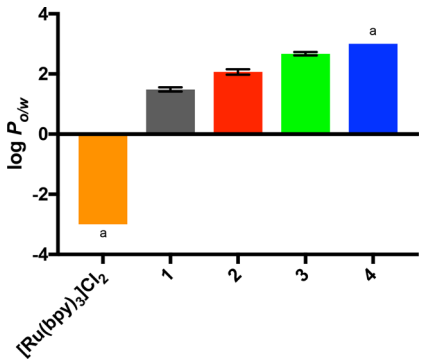

Figure 2. Octanol−water partition coefficients of complexes **1**−**4** as Cl^- salts compared to $[Ru(bpy)_3Cl_2]$. (a) The concentration was too low for detection and was assumed to be <0.1%.

3.3. Photophysical Properties. *3.3.1. Absorption.* Four major types of electronic transitions were apparent in the absorption spectra collected for compounds **1**−**4** in MeCN at room temperature (Figure 3, Table 1). In accordance with

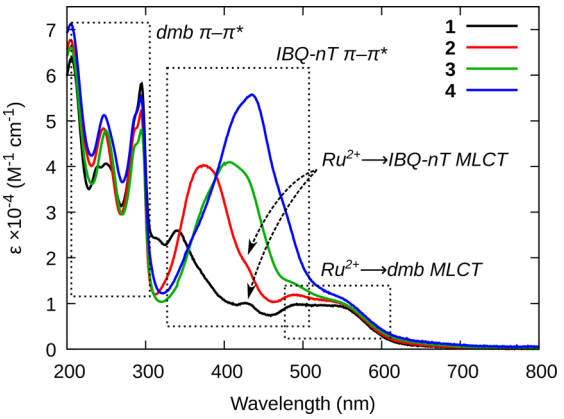

Figure 3. Ground-state absorption spectra of complexes **1**−**4** as their PF_6^- salts in MeCN at room temperature.

Table 1. Electronic Absorption Data for Complexes 1−4

CMPD	λ_{max} absorption (log ε), nm
1	250 (4.61), 295 (4.76), 340 (4.41), 550 (3.97)
2	246 (4.68), 294 (4.72), 374 (4.61), 550 (4.00)
3	248 (4.79), 294 (4.72), 405 (4.78), 550 (3.98)
4	247 (4.71), 294 (4.74), 435 (4.75), 550 (4.05)

earlier assignments for cyclometalated Ru(II) complexes,[15,17] the sharp, intense peaks in the 250−300 nm region were assigned to intraligand (IL), also known as ligand-centered (LC), $\pi\pi^*$ transitions associated with the 4,4′-dmb ligands. The broader bands between 300 and 500 nm, which showed the expected inverse correlation between energy and n, were ascribed to $\pi\pi^*$ transitions localized on the thienyl-containing IBQ-*n*T ligands. The less intense absorption bands in the 500−600 nm region were assigned to MLCT transitions between the Ru(II) center and the 4,4′-dmb ligands. The analogous MLCT transitions between the Ru(II) center and the IBQ-*n*T ligands were largely obscured by overlapping transitions, but a small peak at 425 nm—most discernible in the spectrum of **1**, but also evident as a shoulder in the other spectra—was assigned to the MLCT transition involving the C^N ligands. This state was more energetic than the MLCT state involving the N^N

DOI: 10.1021/acs.inorgchem.8b00689
Inorg. Chem. XXXX, XXX, XXX−XXX

coligands, which is consistent with the elevated C^N-based π^* orbital energy, determined electrochemically for other C^N complexes.[39]

3.3.2. Emission. When excited with light of sufficient energy, all of the Ru(II) C^N complexes produced dual emission at room temperature and at 77 K: blue-green fluorescence from the C^N-based ^{1}IL state and NIR phosphorescence from the N^N-based ^{3}MLCT state (Figure 4, Table 2). To ensure that

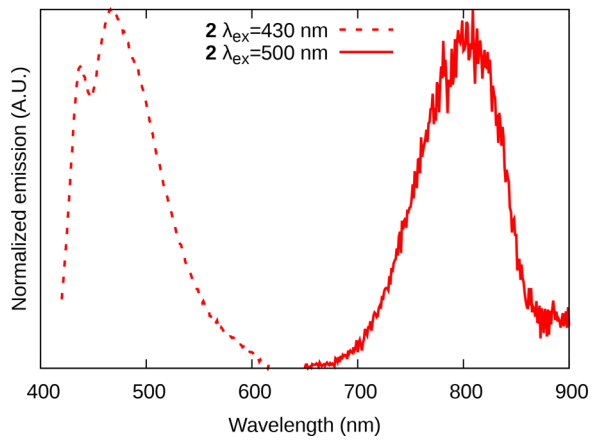

Figure 4. Representative example of dual ^{1}IL and ^{3}MLCT emission from complex **2**.

the ^{1}IL emission was not due to the highly emissive free ligand as a minor contaminant (not observable by other methods), the excitation spectra of the metal complexes and their free ligands were closely scrutinized. Figure S10 compares the excitation spectra collected at three different emission wavelengths (B–D) and the emission spectra (A) for complex **2**, its free ligand IBQ-2T, and complex **2** contaminated with 1% free ligand. The excitation and emission spectra of the pure metal complexes are distinct from their free ligands. With 1% free ligand present, the emission and excitation spectra of the contaminated metal complex are indistinguishable from those of the free ligand (due to the much larger emission quantum yield of the free ligands). Therefore, a comparison of the excitation and emission spectra for free ligands and their metal complexes verifies that the fluorescence observed is produced by the metal-bound ligand.

These transitions could be probed selectively by judicious choice of the excitation wavelength. As expected, the ^{1}IL excitation and emission energies decreased with increasing thiophene chain length, whereas the ^{3}MLCT excitation and emission energies did not depend on the extent of thienyl conjugation in the C^N ligand. UV excitation produced blue ^{1}IL fluorescence from **1** (n = 1), and blue excitation induced green ^{1}IL fluorescence from **4** (n = 4). NIR ^{3}MLCT phosphorescence was observed for all of the complexes, with excitation maxima in the 500–560 nm range and no dependence on the extent of IBQ-nT thienyl conjugation. This information was sufficient to assign the orbital parentage of the IL and MLCT transitions to IBQ-nT $\pi\pi^*$ and $Ru^{2+}(d\pi) \rightarrow$ 4,4′-dmb(π^*), respectively.

Complexes **1**–**4** produced weak ($\Phi_p \approx 10^{-3}$ to 10^{-4}, Table 3), unstructured ^{3}MLCT phosphorescence centered near 800

Table 3. ^{3}MLCT Emission and Singlet Oxygen Quantum Yields[a]

Cmpd	Φ_p ^{3}MLCT (Ar)	Φ_p MLCT (77K)	ΦΔ
1	3.5×10^{-4} (530)	5.8×10^{-3} (530)	0.041 (530)
2	1.7×10^{-4} (500)	9.2×10^{-3} (500)	0.044 (500)
3	2.3×10^{-3} (556)	6.6×10^{-3} (556)	0.066 (556)
4	2.1×10^{-3} (530)	2.6×10^{-4} (550)	0.16 (530)

[a]Excitation wavelengths (nm) are indicated in parentheses.

nm at room temperature in deoxygenated MeCN regardless of the number of thiophenes appended to the C^N ligand, suggesting that the π^* acceptor orbital of the ^{3}MLCT state is likely the same for all four complexes. Thus, the ^{3}MLCT phosphorescence was ascribed to the $Ru^{2+}(d\pi) \rightarrow$ 4,4′-dmb(π^*) state. Compared to the room temperature emission, phosphorescence from compounds **1**–**4** at 77 K (in 4:1 MeOH/EtOH) shifted to shorter wavelengths, increased in intensity, and developed characteristic ^{3}MLCT vibronic structure. The vibronic intervals in the 77 K emission were around 1150–1200 cm^{-1}, which is diagnostic of diimine involvement in the emissive excited state.[40] These observations substantiate that the lowest energy emissive state is MLCT in character and involves $Ru^{2+} \rightarrow$ 4,4′-dmb transitions. This position is supported further by ΔE_s values ranging from 1223 to 1264 cm^{-1}, which is comparable to ΔE_s = 1127 cm^{-1} for $[Ru(bpy)_3]^{2+}$ under the same conditions and is consistent with what would be expected from polar ^{3}MLCT excited states.

The room temperature ^{3}MLCT emission from **1**–**4** in argon-sparged MeCN was very short-lived ($\tau \approx$ 12–18 ns) and comparable to what we reported previously for a related family of Ru(II) cyclometalated systems derived from the IBQ C^N ligand (Table 4).[17] There was no correlation with the number of thienyl rings in the C^N ligand, which agrees with emission originating from the N^N-based ^{3}MLCT. The short ^{3}MLCT lifetimes are not unexpected. For example, the RPC archetype $[Ru(bpy)_3]^{2+}$ has an ^{3}MLCT emission lifetime of around 1 μs,[1] while its cyclometalated $[Ru(bpy)_2(C^N)]^+$ analog has a lifetime of only 12 ns.[15]

The short ^{3}MLCT lifetimes lengthened on going from room temperature to 77 K ($\tau_1 \approx$ 231–256 ns) but were still much shorter than what would be expected for the corresponding

Table 2. ^{1}IL and ^{3}MLCT Emission Maxima Measured for Compounds 1–4 in Argon-Sparged MeCN at Room Temperature or in 4:1 EtOH/MeOH Glass at 77 K[a]

	IL fluorescence			MLCT phosphorescence		
CMPD	λ_{em}, nm (Ar)	λ_{em}, nm (77 K)	ΔE_s, cm^{-1}	λ_{em}, nm (Ar)	λ_{em}, nm (77 K)	ΔE_s, cm^{-1}
1	426 (340)	381 (340)	2773	804 (530)	730 (530)	1261
2	455 (385)	424 (385)	1607	803 (500)	729 (500)	1264
3	495 (405)	465 (405)	1303	804 (556)	732 (556)	1223
4	526 (435)	495 (435)	1191	801 (530)	728 (550)	1252

[a]Excitation wavelengths (nm) are indicated in parentheses.

DOI: 10.1021/acs.inorgchem.8b00689
Inorg. Chem. XXXX, XXX, XXX–XXX

Table 4. Emission and Transient Absorption Lifetimes Measured for Complexes 1−4 in Argon-Sparged MeCN at Room Temperature

	τ_{em} (λ_{em}, nm)		τ_{TA} (λ_{probe}, nm)	
Cmpd	λ_{ex} = 355 nm		λ_{ex} = 355 nm	λ_{ex} = 532 nm
1	9.4 ns (410)	17 ns (810)	7.5 μs (700)	16 ns (700)
2	4.1 ns (450)	17 ns (810)	5.3 μs (600)	17 ns (550)
3	4.2 ns (500)	18 ns (810)	8.1 μs (630)	17 ns (467)
4	4.8 ns (540)	12 ns (810)	7.2 μs (660)	12 ns (487), 3.8 μs (667)

N^N complexes, agreeing with the predictions of the energy gap law (Table S1). An unexpected observation at 77 K was the appearance of an additional lifetime (τ_2) that was influenced by the number of thienyl rings in the C^N ligand and not apparent at room temperature in fluid solution. While τ_2 was similar for **1** and **2** (644 ns versus 557 ns), this lifetime increased to 1.02 μs for **3** and 1.37 μs for **4**. Both 355 and 532 nm excitation produced this additional lifetime and trend over the range of emission wavelengths monitored (720−800 nm). There was no identifying feature in the steady-state 77 K phosphorescence spectra that could be attributed to an additional emissive state, suggesting that the two lifetimes originate from the same N^N-based ^{3}MLCT state. It is unclear why τ_2 was twice as long for compounds **3** and **4** (relative to **1** and **2**) given that their emission profiles and calculated ΔE_s values were very similar (Table 2). The shift of the ^{3}MLCT emission to higher energies at lower temperature may affect the coupling of the N^N-based ^{3}MLCT state to other decay channels that are influenced by the nature of the C^N-based ligand, although this statement is speculative at this point.

3.3.3. Transient Absorption (TA). 3.3.3.1. General Trends. The triplet excited states of Ru(II) C^N complexes **1**−**4** were also probed using nanosecond transient absorption (TA) spectroscopy, and their spectroscopic signatures were analyzed in the context of the well-established TA profiles of prototype Ru(II) N^N complexes,[41] related Ru(II) C^N complexes,[15,39,41,42] as well as Ru(II) N^N dyads containing pyrenyl[43] and oligothienyl[44−47] organic chromophores.

Excited-state absorption (ESA) spectra are differential measurements that superimpose lost ground state absorptions with new absorptions associated with the excited-state chromophore. The TA signature of RPCs generally involves three principal features: a net absorption in the near-UV, a strong bleach in the mid-visible, and a very broad but weak absorption extending into the red and NIR.[41] For Ru(II) N^N complexes in particular, the bleach in the midvisible corresponds to the loss of the $^1A_1 \rightarrow {}^1$MLCT ground-state absorption upon formation of the excited state. The positive signals in the near-UV and in the red/NIR correspond to ESA by the diimine ligand radical anion of the ^{3}MLCT excited state. The red/NIR absorption also has contributions from ligand-to-metal charge transfer (LMCT) transition(s) involving ancillary N^N ligands. This longer wavelength transient is generally broad and featureless, and of very low intensity due to the overlap of the negative signal from the ground state charge-transfer bleach with these inherently weak ESA signals.

The transient absorption spectra for complexes **1**−**4** were recorded from 350−750 nm at various time delays after the laser pulse with excitation at 355 and 532 nm (Figures S11−S19). Excitation at the shorter wavelength gave rise to a prominent ground-state bleach in the midvisible region at zero time delay that decayed with a time constant on the order of 13−17 ns, which agreed very well with the 12−17 ns emission lifetimes measured at 810 nm (Table 4). Therefore, the TA transient observed immediately after the excitation pulse was ascribed to the NIR-emissive ^{3}MLCT state for all of the compounds. The TA signature of this zero-time-delay transient across the entire wavelength region probed agreed very well with what is known for RPCs with ^{3}MLCT excited states for complexes **1** and **2**. However, complexes **3** and **4** displayed a positive signal in the red/NIR that was much sharper and of greater intensity than what is normally attributed to LMCT and diimine radical ligand−radical anion transitions in the corresponding Ru(II) N^N complexes. This positive transient was detected for all of the Ru(II) C^N complexes at long delay times, albeit weakly in **1** and **2**.

Decay of this short-lived ^{3}MLCT state revealed a positive transient with a much longer lifetime (τ_{TA} = 4−8 μs) that was not detected in the emission measurements (Figure 5A). The

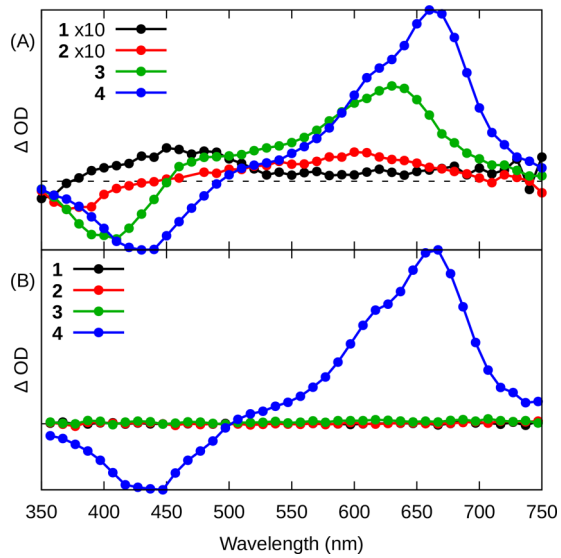

Figure 5. Transient absorption spectra collected for complexes **1**−**4** with λ_{pump} = 355 nm (A) or 532 nm (B) at a delay time of 90 ns with 10 ns integration. The traces for compounds **1** and **2** in A are multiplied by 10 for clarity.

maximum positive signal of this transient red-shifted and became more intense on going from **1** to **4** (i.e., with increasing number of thiophene rings). On the basis of the intense absorptive features and the microsecond lifetimes that resembled the TA signatures of the free ligands as well as published Ru(II) N^N systems incorporating oligothiophenes,[44−47] the long-lived TA state was assigned as ^{3}IL for all the compounds (Scheme 1A). Generally, the ^{3}IL lifetimes for the complexes were somewhat shorter than those measured for the $^3\pi\pi$ states of the free ligands, presumably due to increased ISC facilitated by Ru(II) in the metal complexes. There could also be some mixing with ^{3}MLCT and other charge-transfer excited states (e.g., intraligand charge transfer (^{3}ILCT) and ligand-to-ligand charge transfer (^{3}LLCT)). These microsecond-scale ^{3}IL lifetimes were also shorter than those measured for the corresponding π-expansive Ru(II) N^N complexes,[43,48−51] supporting the position that the ^{3}IL states of

DOI: 10.1021/acs.inorgchem.8b00689
Inorg. Chem. XXXX, XXX, XXX−XXX

Scheme 1. Jablonski Diagrams Depicting Excited State Relaxation Pathways for Complex 3 with 355 (A) or 532 nm (B) Excitation

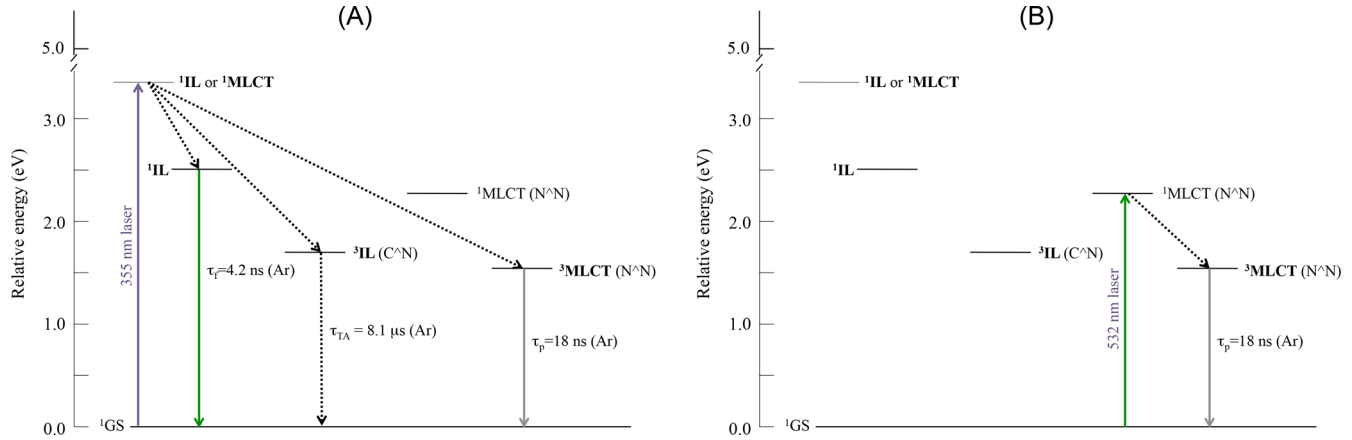

the Ru(II) C^N complexes in this study have some contributing ^{3}MLCT character (^{3}MLCT lifetimes are shorter for Ru(II) C^N complexes than for Ru(II) N^N complexes) and/or increased ^{3}LLCT character (Ru(II) C^N complexes have a significant amount of ligand character in the HOMO).

Excitation at 532 nm precluded access to the nonemissive, long-lived ^{3}IL state for complexes **1**−**3**, and only the short-lived ^{3}MLCT transient signal was observed. Compound **4**, however, showed the short-lived ^{3}MLCT decay as well as an intense positive transient with a 2−4 μs lifetime with the longer wavelength excitation (Figure 5B, Scheme 1B). The major difference between complexes **1**−**3** and **4** is that both ^{1}IL and ^{1}MLCT states should be accessible with 532 nm excitation for **4** (Scheme 2), whereas only ^{1}MLCT states are accessible for **1**−**3**.

Scheme 2. Simplified Jablonski Diagram Depicting Excited State Relaxation Pathways for Complex 4 with 532 nm Excitation

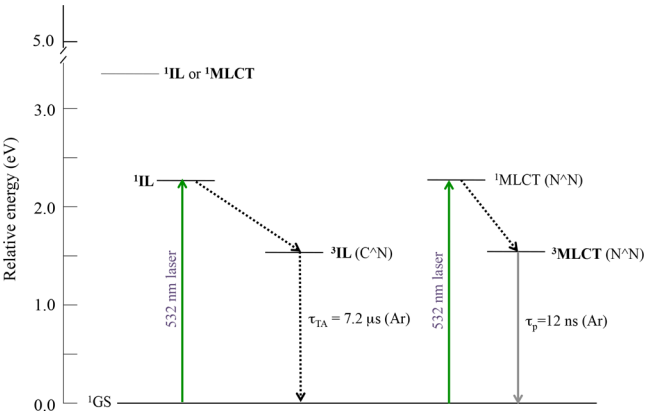

On the other hand, 355 nm excitation can populate higher-energy excited states that relax through both ^{3}MLCT and ^{3}IL pathways in all four complexes.

The C^N-based ^{3}IL energies for complexes **2**−**4**, estimated to be slightly less than the triplet state energies of the free α-oligothiophenes,[52] are expected to be below that of the ^{1}MLCT accessed with 532 nm excitation, making it energetically feasible for the ^{1}MLCT state populated under these conditions to relax to lower-lying C^N ^{3}IL states. However, **4** is the only compound where the ^{3}IL state can be populated with 532 nm excitation, as evidenced by the long-lived transient with a very prominent red/NIR ESA (Figure 5B). Likewise, **4** is the only compound where the ^{1}IL states are low enough in energy to be directly populated by 532 nm excitation. It may be the case that intersystem crossing (ISC) between states of similar character is faster than ISC between MLCT and IL states, which would explain why the ^{3}IL transient is only observed with excitation energies where ^{1}IL states are directly accessible (namely, 355 nm for all complexes, and 532 nm only in the case of **4**). Another plausible explanation is that ISC from the ^{1}MLCT to the ^{3}IL (not depicted in Scheme 2) may occur when these states are similar in energy or when the ^{3}IL state is lower in energy than the ^{3}MLCT state, which is also only possible for **4**. We discounted the possibility of internal conversion (IC) from the ^{3}MLCT state to the ^{3}IL state because no rise time for the ^{3}IL TA signal matching the ^{3}MLCT decay time was detected.

The photophysical models put forth in Schemes 1 and 2 are preliminary and serve as a starting point for understanding the differences in the excited state dynamics of the Ru(II) complexes with π-expansive C^N ligands observed at two different excitation wavelengths. A much more quantitative photophysical analysis with respect to the relative energies, coupling, and equilibria (if any) between the ^{3}IL and ^{3}MLCT states is required to understand these systems in the same detail that has been established for Ru(II) complexes containing π-expansive N^N ligands (notably, those derived from pyrene).[43,53−61]

3.3.3.2. Detailed Kinetics by Compound. When **1** was excited at 532 nm in argon-saturated MeCN, the TA spectrum obtained at zero time delay (Figure 6B) was reminiscent of that described for RPCs,[41,62] except that the maximum negative signal for the ground state bleach occurred near 550 nm, while it was around 475 nm for the corresponding N^N complex. This is consistent with the ground-state absorption maxima for Ru(II) C^N complexes being red-shifted by about 100 nm, compared to the Ru(II) N^N counterpart.

When **1** was excited at 355 nm in argon-saturated MeCN, the TA spectrum obtained immediately after the excitation pulse was qualitatively similar to that obtained with 532 nm except that the ground-state bleach signal near 410 nm appeared stronger (Figures 6A, S11−S12). At longer times, however, the shorter 355 nm excitation produced a broad ESA centered near 425 nm with a much longer lifetime (τ = 3.8 μs). This longer-

DOI: 10.1021/acs.inorgchem.8b00689
Inorg. Chem. XXXX, XXX, XXX−XXX

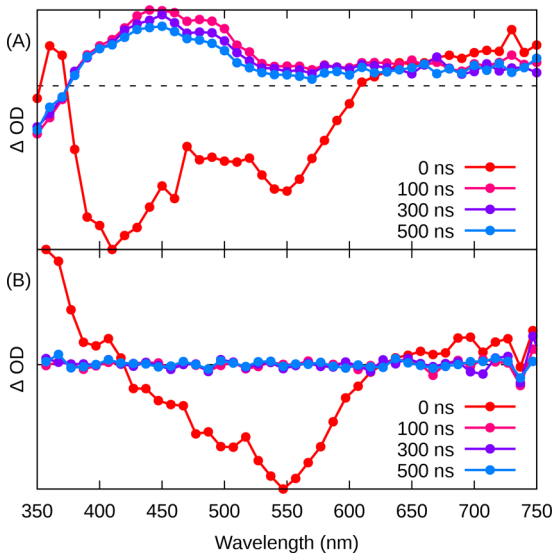

Figure 6. Comparison of the transient absorption decays for Ru(II) C^N complex **1** collected with λ_{pump} = 355 nm (A) or 532 nm (B). Slices are 100 ns wide, beginning at the indicated time.

lived TA state that was not observed in the phosphorescence measurements or the TA spectra collected with λ_{ex} = 532 nm is tentatively assigned to a C^N-based ^{3}IL state of $^3\pi\pi^*$ character that is inferred to be of higher energy than the ^{3}MLCT state(s) since it was not accessible with 532 nm excitation.

Complex **2** behaved in a similar manner to complex **1**. With both 532 and 355 nm excitation, the zero time delay TA spectra for **2** resembled what would be expected from a typical ^{3}MLCT excited state of an RPC (Figure S13). The transient produced with 532 nm excitation decayed monoexponentially at 550 nm with a time constant of 17 ns, and no long-lived ESA was detected. However, excitation with higher photon energies (λ_{ex} = 355 nm) revealed a broad, positive ESA centered near 600 nm with a monoexponential lifetime of 5.3 μs (Figure S14). Assignment of this longer-lived state as the ^{3}IL was confirmed by comparing the TA signature of **2** with that for the free ligand IBQ-2T using λ_{ex} = 355 nm (Figure 7). There were only minor differences between the shapes of their normalized TA spectra, but the lifetime of the free IBQ-2T ligand was longer with

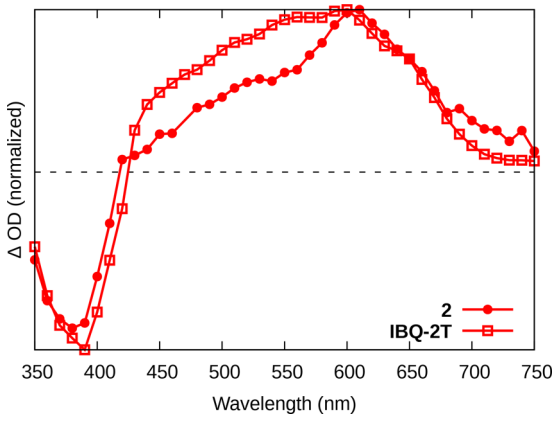

Figure 7. Comparison of the transient absorption spectra (λ_{pump} = 355 nm) for Ru(II) C^N complex **2** as its PF_6^- salt in MeCN and the corresponding free ligand IBQ-2T in DMSO. The integration time for IBQ-2T was 0–20 μs and for 2 it was 0–1 μs.

multiexponential kinetics at 600 nm (τ_{TA} = 25, 106 μs). The shortened ^{3}IL lifetime of **2** relative to that of its free ligand is most likely due to increased ISC in the Ru(II) C^N complex due to the presence of the heavy metal atom, although contributions from states with ^{3}ILCT and ^{3}LLCT or ^{3}IL/^{3}MLCT mixing could also play a role.

Complex **3** also followed the trend observed for **1** and **2** in that 532 nm excitation yielded a single, monoexponential decay with a time constant of 17 ns at 467 nm, while 355 nm excitation gave rise to a long-lived excited state (Figures S15, S16). The only notable difference was that 355 nm excitation of **3** produced an ^{3}IL state that was much more absorptive, which significantly attenuated the ground state bleach in the 475–550 nm region. Its triplet excited-state lifetime estimated from the decay of the positive TA transient at 630 nm was 8.1 μs, but a double exponential fit using τ_{TA} = 5.4 and 11 μs described the data more accurately. The lifetime of the free IBQ-3T ligand was also long and was best described by multiexponential kinetics at 650 nm (τ_{TA} = 4, 39 μs). Again, increased ISC can explain the shorter mean ^{3}IL lifetime for the Ru(II) C^N complex.

Complex **4** behaved very differently from the other three compounds. At zero-time-delay with both 355 and 532 nm excitation, the transient signal for **4** showed a prominent ESA characteristic of the ^{3}IL state superimposed on a ground-state bleach that decayed with a time-constant of 12–14 ns at 550 nm (Figures S17–S19) and agreed with the emissive ^{3}MLCT state lifetime. The sharp and intense ^{3}IL ESA was centered near 675 nm with lifetimes of 7.2 μs (λ_{pump} = 355 nm, λ_{probe} = 660 nm) or 3.8 μs (λ_{pump} = 532 nm, λ_{probe} = 667 nm) that did not correspond to τ_{em}. The shorter value for τ_{TA} observed with 532 nm excitation may reflect differences in the nature of the TA states formed with different excitation wavelengths. Regardless, the shorter ^{3}IL lifetimes compared to those of the analogous Ru(II) N^N complexes are consistent with increased ISC in the C^N complexes and possibly mixing with the much shorter-lived ^{3}MLCT states.

3.3.4. Singlet Oxygen Sensitization. Quantum yields for singlet oxygen generation (Φ_Δ) by **1**–**4** were measured in air-saturated MeCN solution by probing sensitized $^1O_2$ luminescence centered at 1268 nm (Table 3). These yields are estimates because the luminescence from $^1O_2$ overlapped with the ^{3}MLCT phosphorescence. Compared to $[Ru(bpy)_3](PF_6)_2$ (Φ_Δ = 0.56),[26] which is an efficient singlet oxygen sensitizer, the Ru(II) C^N complexes of this study were not as effective. Upon excitation of the ^{1}MLCT transition (λ_{ex} = 500–560 nm), complexes **1** and **2** sensitized $^1O_2$ with a quantum yield on the order of 4%, while **3** was slightly higher at 7%. The capacity for generating singlet oxygen appeared to increase with the number of thiophenes in the IBQ-*n*T ligand, with complex **4** yielding 16%. When the excitation wavelength was shortened to reflect the excitation maxima for the ^{1}IL transition, these singlet oxygen quantum yields increased to 15–32%, with complexes **3** and **4** being very similar. The excitation wavelength dependence of Φ_Δ indicates that initial population of the ^{1}IL state may be more effective at producing singlet oxygen than the ^{1}MLCT state. Regardless, these values are much smaller than the $^1O_2$ quantum yields measured for the analogous RPCs.[20] For example, Φ_Δ measured for $[Ru(4,4'\text{-dmb})_2(IP\text{-}n\text{T})]Cl_2$ (where n = 1–4) increased from 50 to 100% on going from n = 1 to 4. The much lower efficiencies for $^1O_2$ generation in the case of the cyclometalated Ru(II) compounds can be attributed to an excited state decay that is heavily influenced by the ^{3}MLCT

DOI: 10.1021/acs.inorgchem.8b00689
Inorg. Chem. XXXX, XXX, XXX–XXX

Table 5. (Photo)toxicities of Complexes 1−4 towards SK-MEL-28 Cells and Selectivity Factors for SKMEL28 Cancer Cells Compared to Normal Human Skin Fibroblasts

	dark		vis light		red light	
	EC_{50} (μM)	SF	EC_{50} (μM)	PI	EC_{50} (μM)	PI
1	0.51 ± 0.04	30	0.18 ± 0.05	2.8	0.22 ± 0.07	2.3
2	0.38 ± 0.03	53	0.15 ± 0.04	2.5	0.29 ± 0.02	1.3
3	5.11 ± 0.08	59	0.12 ± 0.01	43	0.72 ± 0.26	7.1
4	>300	-	0.26 ± 0.02	>1153	16.6 ± 1.53	>18

energy, whereby nonradiative decay completes effectively with $^1O_2$ sensitization and phosphorescence.

3.4. Photobiological Activity. *3.4.1. Cytotoxicity and Photocytotoxicity.* Compounds **1**−**4** were assessed in SKMEL28 melanoma cells and CCD-1064Sk normal human skin fibroblasts for their cytotoxic effects in the absence of a light trigger (Table 5, Figure 8). The cytotoxicities of the

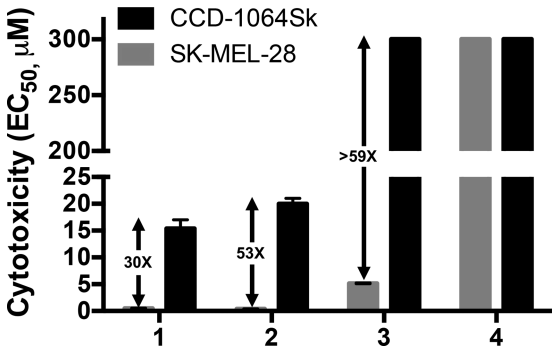

Figure 8. Comparison of the dark cytotoxicities toward SK-MEL-28 and CCD-1064Sk cells for complexes **1**−**4**.

Ru(II) C^N compounds toward these two cell lines did not correlate with their lipophilicities. In fact, cytotoxicity generally decreased with lipophilicity. This observation stands in contrast to the widely reported notion that increased hydrophobicity leads to increased cellular uptake, which, in turn, enhances cytotoxicity. In fact, we often observe the opposite: decreased cytotoxicity for π-expanded systems with increased lipophilicity. We believe there are two primary reasons: (1) π-expanded systems can aggregate at the extracellular surface, which reduces cellular uptake (until a light trigger causes photoactivated uptake), and (2) nuclear uptake, which may be an important factor governing cytotoxicity, often decreases with increased lipophilicity (vide infra).

Compounds **1** and **2** were highly cytotoxic toward melanoma cells with submicromolar potencies (EC_{50} = 0.51 and 0.38 μM, respectively), while **3** was approximately 10-fold less cytotoxic (EC_{50} = 5.1 μM). All three compounds were selectively cytotoxic toward melanoma cells over normal skin fibroblasts, with SFs ranging from 30 to almost 60 (Figure 8). Notably, compound **4** was completely nontoxic (EC_{50} > 300 μM) to both cell lines, defying the conventional view that cyclometalated Ru(II) complexes are inherently more cytotoxic than their diimine counterparts. For comparison, compounds **1** and **2** were more than 5× more potent than cisplatin toward melanoma cells, with cisplatin exhibiting no selectivity toward melanoma cells (EC_{50} = 2.8 μM in SKMEL28; EC_{50} = 2.6 μM CCD-Sk1064).

In terms of structure−activity relationships, it is interesting to note the striking difference between the cytotoxic profiles of compounds **3** and **4**, which differ by only one thienyl group. This marked change from potent chemotherapeutic (toward melanoma cells) to nontoxic agent (and potential photosensitizer) on going from three thienyl groups to four is reminiscent of what we previously observed for a cyclometalated Ru(II) family of compounds based on the phenazine-derived C^N ligand framework.[17] In this series, the fusion of just one additional benzene ring to the pbpz ligand to yield the more π-expansive pbpn reduced cytotoxicities by more than 150-fold in SKMEL28 cells and almost 270-fold in HL60 cells. In fact, the cyclometalated $[Ru(bpy)_2(pbpn)]Cl$ complex was slightly less cytotoxic than the corresponding diimine $[Ru(bpy)_2(dppn)]Cl_2$. Importantly, π-extension on the C^N ligand was a requirement as the related $[Ru(bpy)(phpy^-)(dppn)]Cl$ acted as a traditional cytotoxin.[19] The observation of an abrupt change in cytotoxicity at a critical degree of π-extension in a second Ru(II) C^N series supports our previous correction to the existing dogma that Ru(II) C^N complexes are inherently more cytotoxic than their N^N counterparts. π-Extended C^N ligands appear to play an important role in reducing the toxicities of the cyclometalated Ru(II) systems.

The photocytotoxicities of the cyclometalated Ru(II) complexes toward melanoma cells were determined using visible or red light and compared to their dark cytotoxicities (Table 5, Figures 9 and S20). The photocytotoxicities toward

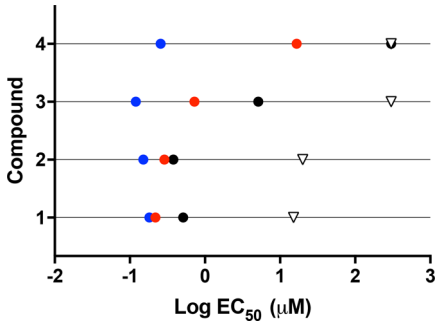

Figure 9. Cytotoxic activity plot for compounds **1**−**4** against SK-MEL-28 melanoma cells (filled circles) and CCD-1064Sk (open triangles) with the following treatment conditions: dark (black), blue (visible light), or red (red light). Only the dark condition is shown for CCD-1064Sk.

CCD-1064Sk cells are not reported because this cell line was sensitive to the light treatment without added compound. The fluence for light-treated melanoma cells was 100 J cm^{-2} delivered at a rate of 28 or 35 mW cm^{-2} for visible and red light, respectively. All of the compounds exhibited similar photocytotoxicities at submicromolar concentrations upon visible light activation, with EC_{50} values ranging from 120 nM for **3** to 260 nM for **4**. However, their PIs differed markedly. The PIs for **1** and **2** were less than 3, owing to the baseline cytotoxicity associated with these particular structures,

DOI: 10.1021/acs.inorgchem.8b00689
Inorg. Chem. XXXX, XXX, XXX−XXX

and thus they are not considered photosensitizers for phototherapy. The slightly reduced cytotoxicity of **3** led to a PI greater than 40 but still much smaller than what would be expected from the corresponding Ru(II) N^N system. Compound **4**, in contrast, proved to be an excellent photosensitizer with a PI exceeding 1100 (Figures 10 and S20).

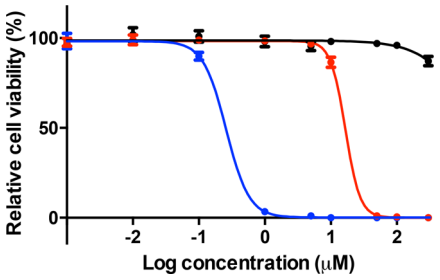

Figure 10. In vitro dose–response curves for SK-MEL-28 melanoma cells treated with complex **4** in the dark (black) or with visible (blue) or red (red) light activation.

As was the case for broadband visible light, monochromatic red light (625 nm) produced very few (if any) phototherapeutic effects on melanoma cells treated with compounds **1** and **2**. This was not surprising given the dark cytotoxicity associated with these compounds and the lower photon energy for red light. The PI for **3** dropped from 43 to 7 with red light, and from over 1100 to 18 for **4** despite the stronger absorption of red light characteristic of Ru(II) C^N complexes ($\varepsilon \approx 2400$ M^{-1} cm^{-1} for **4** versus 100 M^{-1} cm^{-1} for the corresponding N^N complex at 625 nm).

The low PIs for compounds **1** and **2** and the marginal PI for **3** indicate that photons do not significantly amplify their inherent cytotoxic activities. The thousand-fold phototherapeutic margin for **4** with visible light is attributed to an absence of dark cytotoxicity for this more π-expansive complex combined with a highly photosensitizing, low-lying ^{3}IL state that is in energetic proximity to or lower in energy than the N^N-based ^{3}MLCT (<1.5 eV). The TA experiments showed that this ^{3}IL state is accessible with excitation in the visible range as demonstrated by the 3.8 μs intrinsic lifetime obtained with λ_{ex} = 532 nm. However, the attenuated PI for red light suggests that red absorption may preferentially populate MLCT states that decay very rapidly (τ_{em}, τ_{TA} = 12 ns), precluding access to the long-lived ^{3}IL state that is extremely sensitive to excited state quenchers.

This argument is supported by the much larger red PI value measured for the corresponding Ru(II) N^N complex, where the ^{3}MLCT state lies well above the low-energy ^{3}IL state thought to be responsible for potent photobiological effects. For the Ru(II) diimine complex, ^{3}IL states may be directly populated with 625 nm excitation, albeit with low oscillator strengths owing to the forbidden nature of this transition,[20,63] or accessed from direct population of the higher-lying ^{3}MLCT with an intrinsic lifetime approximately 100× longer than the cyclometalated system. The longer-lived ^{3}MLCT may also contribute to in vitro photocytotoxic effects in this case.

Regarding the source of the PDT (and/or PCT) effects observed for **3** and **4**, cell-free $^1O_2$ quantum yields were extremely low (vide supra). Other parameters, such as redox potentials, were not determined as part of this study. The metal-based oxidation potentials are expected to be modest as demonstrated for a variety of Ru(II) C^N complexes that lack electron-withdrawing groups on the auxiliary ligands.[15,29] Therefore, excited state oxidation of biological substrates by the metal seems unlikely. Dissociative metal-centered d$\pi \rightarrow$ dσ^* states are inaccessible from the lower-energy ^{3}MLCT states characteristic of the cyclometalated Ru(II) systems, so covalent modification of biological substrates following photoinduced ligand loss is also not a viable pathway. Our current hypothesis is that redox processes centered on the α-oligothienyl unit may play a role in the excited state reactivity of this series, especially **3** and **4**. MacDonnell/Wolf and co-workers previously reported long-lived charge separated states in Ru(II) complexes with bithienyl-functionalized ligands, whereby the role of the bithienyl group is to reductively quench the Ru(III) formed upon photoexcitation.[44,64,65] The result is a long-lived ^{3}ILCT excited state ($\tau_{em} \approx 7.4$ μs) with the hole (h^+) localized on bithiophene. This state was proposed to have a large amount of stored energy ($\Delta G^\circ \approx 2.0$ eV). Whether this reasoning can be applied to Ru(II) C^N ligands functionalized with α-oligothienyl units remains to be determined.

3.4.2. Preliminary Mechanistic Studies. DNA Interactions. Disruption of the topological structure of DNA is a known cytotoxic mechanism. Therefore, the abilities of the Ru(II) C^N complexes to interact with DNA in a cell-free environment were probed by an established gel mobility-shift assay (Figure 11).[66–68] Briefly, pUC19 plasmid DNA was dosed with

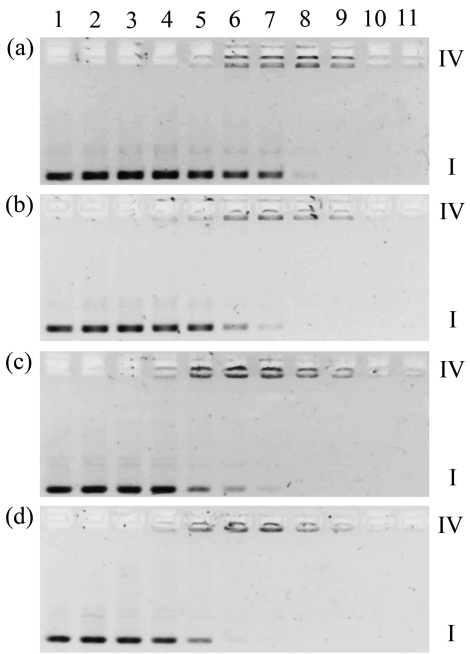

Figure 11. DNA gel mobility shift assays of pUC19 DNA (20 μM bases) dosed with metal complex (MC) **1** (a), **2** (b), **3** (c), or **4** (d) and visible light (14 J cm^{-2}, 7.8 mW cm^{-2}). Lane 1, DNA only (-*hν*); lane 2, DNA only (+*hν*); lane 3, 5 μM MC (+*hν*); lane 4, 10 μM MC (+*hν*); lane 5, 15 μM MC (+*hν*); lane 6, 20 μM MC (+*hν*); lane 7, 25 μM MC (+*hν*); lane 8, 30 μM MC (+*hν*); lane 9, 35 μM MC (+*hν*); lane 10, 40 μM MC (+*hν*); lane 11, 40 μM MC (-*hν*).

increasing concentrations of **1**–**4** and exposed to a visible light treatment (lanes 2–10) alongside controls of DNA not treated with metal complex with or without light treatment (lanes 1 and 2), and DNA dosed with the highest concentration of metal complex and not exposed to light (lane 11). The dose–response profiles of **1**–**4** in the presence of pUC19 plasmid DNA were very similar. The unifying feature for all complexes

DOI: 10.1021/acs.inorgchem.8b00689
Inorg. Chem. XXXX, XXX, XXX–XXX

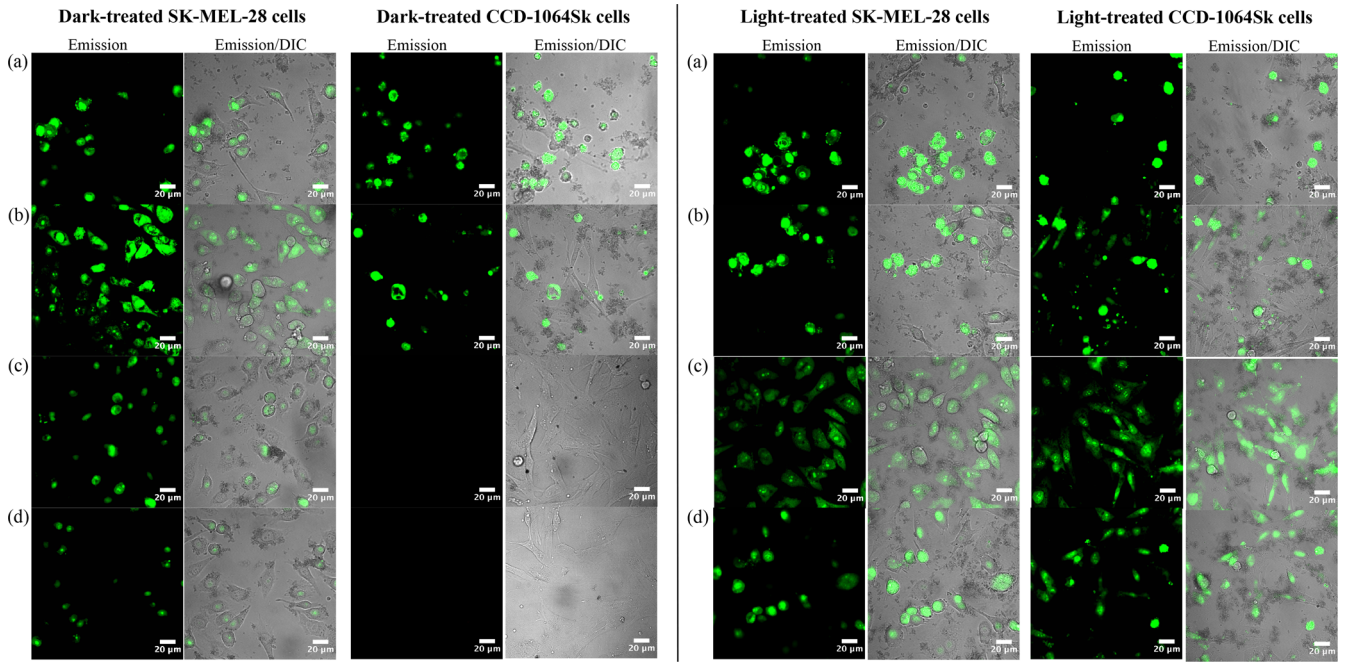

Figure 12. Laser-scanning confocal microscope images of SK-MEL-28 melanoma cells or CCD-1064Sk normal skin fibroblasts treated with compounds **1** (a), **2** (b), **3** (c), or **4** (d) at 25 μM and kept in the dark (left panel) or exposed to a 50 J cm^{-2} (35 mW cm^{-2}) visible light treatment (right panel). Scale bar = 20 μm.

was the conversion of the form I supercoiled DNA to aggregated form IV DNA. At high concentrations of metal complex, the form IV DNA bands were barely visible on the gel.

Form I DNA represents undamaged plasmid DNA whose topology has not been altered by the metal complex or its treatment with light. As a result, it migrates the farthest on the gel (brighter band at the bottom of the gel in Figure 11). On the other hand, form IV DNA aggregates barely move from the gel loading well (faint band at the top of the gel in Figure 11). No evidence of form II or III, representing DNA with single-strand breaks and double-strand breaks, respectively, was discerned at metal complex-to-nucleotide ratios (r) between 0.25 and 2. Rather, all of the metal complexes facilitated DNA aggregation in a dose-dependent manner. Drug-induced DNA catenation/aggregation has been proposed as a viable cytotoxic mechanism and could be implicated for any metal complex in the present series that accumulates in the nucleus or mitochondria.[69]

The complexes also suppressed fluorescence from ethidium bromide, the intercalating dye used to visualize DNA bands, with or without a light treatment at higher concentrations. In general, nonfluorescent ethidium bromide in the presence of DNA can be attributed to (i) a distorted DNA helix made inaccessible to ethidium by metal-complex binding, (ii) blocking of ethidium DNA intercalation by bound metal complex, or (iii) quenching of ethidium fluorescence by the metal complex. In the present case, the aggregated DNA may lack exposed intercalative sites for ethidium binding. Disruption of DNA binding, especially in processes that are critical for normal cellular function, is a possible cytotoxic mechanism.

The main difference between the DNA interactions of complexes **1**−**4** was the r value at which form I DNA was no longer discernible and form IV was apparent: 1.5, 1.25, 1.25, and 1.0 for **1**−**4**, respectively. These slight differences may highlight a stronger interaction with DNA with increasing π-expansion, but the preference is only marginal and cannot explain the differences in dark cytotoxicity. The gel electrophoretic patterns for **1** and **4** are strikingly similar, yet **1** is highly cytotoxic toward melanoma cells (EC_{50} = 0.51 μM) and **4** is not (EC_{50} > 300 μM). Given that all four Ru(II) C^N complexes disrupt the topological structure of plasmid DNA in a similar manner and at similar concentrations, access to cellular DNA may be the determining factor for dark cytotoxicity within the series.

The substantial difference in cytotoxicity between **1**−**3** and **4** could be related to differences in nuclear accumulation rather than any fundamental difference in their DNA interaction modes in the cell-free environment. Puckett and Barton reported that nuclear accumulation increased as lipophilicity decreased for a small family of Ru(II) dppz complexes incorporating auxiliary ligands of varying hydrophobicity.[38,70] This finding was corroborated for a related family of Ru(II) dppz complexes whereby hydrophobicity was varied by the substituent on the dppz ligand.[71] If lipophilicity is inversely correlated with nuclear accumulation in the present series, increased nuclear accumulation may explain the greater cytotoxicity exhibited by **1** and **2**, the Ru(II) complexes containing less π-expansive C^N ligands. Cellular imaging was used to examine this assertion.

Cellular Imaging. The ^{1}IL emission from the complexes served as a convenient tool for monitoring their cellular uptake and localization by confocal microscopy in an effort to understand better their cytotoxicity and photocytotoxicity profiles (Figure 12). Both melanoma and normal skin fibroblasts were treated with compounds **1**−**4** and observed in the dark and after a sublethal visible light treatment. Overlays of differential interference contrast (DIC) and confocal microscopy images were used to outline cellular morphology and ascertain cellular uptake and localization/distribution at t = 1 h for both dark- and light-treated samples.

DOI: 10.1021/acs.inorgchem.8b00689
Inorg. Chem. XXXX, XXX, XXX−XXX

If it is assumed that the emission signal from the metal complex is proportional to its concentration in all regions of the cell, then several general trends among the four compounds in the dark condition (Figure 12, left panel) emerged: (i) Cellular uptake in the melanoma cell line was greatest for **1** and **2**, less for **3**, and least for **4**. (ii) There was no cellular uptake of **3** and **4** by normal fibroblasts, which remained healthy in appearance. (iii) Uptake of **1** and **2** by normal fibroblasts appeared to be limited to dead and dying cells, and (iv) nuclear accumulation was detectable for all complexes in melanoma cells but decreased on going from **1** to **4**.

Despite the assumption that increased lipophilicity leads to enhanced cellular uptake, the opposite trend was observed for melanoma cells. Cellular uptake decreased on going from **2** to **4**, with **1** and **2** being similar. As was observed by others, nuclear accumulation in the present series was inversely correlated to lipophilicity. However, the reason may not be the same; decreased nuclear accumulation for **3** and **4** could simply be due to decreased cellular uptake. The absence of a fluorescence signal for compounds **3** and **4** in normal fibroblasts and the reduced signal in healthy fibroblasts for **1** and **2** supports the selectivity for melanoma cells over normal skin fibroblasts reflected in the SF values calculated from cytotoxicity experiments.

When cells were treated with compound **1** or **2** and then irradiated, the images captured looked very similar to those collected without irradiation (except that the fibroblasts in particular looked less healthy). This marginal difference between the dark and the light condition was expected given the very small PIs measured for **1** and **2** in the cellular assays. The most striking difference was that between the dark- and light-treated melanoma cells for compounds **3** and **4**, where the fluorescence increased substantially under the light conditions along with a loss in cell viability inferred from the change in cellular morphology from dendritic to detached spherical. These results are also in agreement with the larger PIs measured for **3** and **4**, except that the larger light fluences and longer observation times used in the cell-based assays resulted in much better phototherapeutic effects with **4**. The reason the softer light doses and shorter observation times were used for imaging was to be able to discern nuclear accumulation before cellular morphology was compromised.

Another major difference between the dark and light conditions was that compounds **3** and **4** were taken up effectively by normal skin fibroblasts when treated with light, whereas in the dark they were not. With light treatment, there was no inherent selectivity for melanoma cells over normal skin fibroblasts. This important observation suggests that photoactivated uptake of compounds **3** and **4** can result in very potent, broadly applicable phototherapeutic effects. However, the PI for **3** was only 43 for melanoma cells due to its higher dark cytotoxicity. Compound **4**, on the other hand, had a PI > 1100 and emerged as the lead phototherapeutic compound from this small family. In this case, selectivity for melanomas over healthy cells would be achieved by confining the light treatment to diseased tissue, which is the basis of current PDT. In other words, selective photocytotoxicity toward cancer cells is not a requirement and could potentially limit the broad applicability of PDT to other cancer types.

4. SUMMARY AND CONCLUSIONS

Four cyclometalated Ru(II) complexes were prepared and fully characterized. These new compounds systematically vary the π-conjugation of the C^N ligand by increasing the number of thienyl groups appended to the IBQ ring system on going from **1** to **4**. To our knowledge, this is the second investigation of tris-bidentate Ru(II) cyclometalated systems that incorporate π-expansion on the C^N framework rather than on the auxiliary N^N ligands. As expected, the Ru(II) C^N complexes were considerably more lipophilic than their N^N counterparts, and lipophilicity within the series increased with the number of thienyl groups. The compounds exhibited C^N-based IL fluorescence that decreased in energy with π-conjugation as well as N^N-based MLCT phosphorescence that was independent of π-conjugation on the C^N ligand. The compounds also exhibited nonemissive ^{3}IL states that could be accessed with 355 nm excitation, but only in the case of compound **4** could this state be accessed with 532 nm excitation.

Compounds **1**−**3** were cytotoxic to melanoma cells in the dark, setting an upper limit to the phototherapeutic effects that could be obtained with visible and red light activation. However, they were selectively cytotoxic to melanoma cells over normal skin fibroblasts by 30- to 60-fold, making them selective chemotherapeutic agents. For **1** and **2**, this potency was in the nanomolar regime, and for **3**, it was 5 μM. Compound **4** was completely nontoxic to both melanoma cells and normal skin fibroblasts, but became a powerful in vitro phototherapeutic agent with visible light activation. The cytotoxicity profiles of the Ru(II) C^N complexes toward both cell lines could be qualitatively related to cellular uptake and nuclear accumulation (and possibly facilitation of DNA aggregation with nuclear accumulation) by monitoring the intrinsic IL fluorescence from the C^N ligand of the complexes with confocal microscopy. Photoactivated uptake appeared to be the primary driver of the larger PIs for **3** and **4**, with **4** having an exceptionally large PI (>1100). From a very small family of new Ru(II) C^N complexes, the present study has identified both a potent chemotherapeutic agent (**3**) and a potent phototherapeutic agent (**4**). In addition, compound **4** provides a second example that serves as an exception to the previously held notion that Ru(II) cyclometalated compounds are inherently cytotoxic and thus not acceptable PDT agents. The study also highlights that accessible ^{3}IL states in π-expansive Ru(II) C^N complexes such as **4** are highly photosensitizing, as has been demonstrated for the corresponding N^N complex.

■ ASSOCIATED CONTENT

Ⓢ Supporting Information

The Supporting Information is available free of charge on the ACS Publications website at DOI: 10.1021/acs.inorgchem.8b00689.

1D ^{1}H and 2D ^{1}H−^{1}H COSY NMR spectra for cyclometalating ligands and their corresponding Ru(II) complexes, transient absorption decay spectra for the Ru(II) C^N complexes, cytotoxicity and photocytotoxicity dose−response curves for the Ru(II) C^N complexes (PDF)

■ AUTHOR INFORMATION

Corresponding Authors

*E-mail: cgcamero@uncg.edu.
*E-mail: samcfarl@uncg.edu.

DOI: 10.1021/acs.inorgchem.8b00689
Inorg. Chem. XXXX, XXX, XXX−XXX

ORCID
Sherri A. McFarland: 0000-0002-8028-5055

Notes

The authors declare no competing financial interest.

■ ACKNOWLEDGMENTS

Research reported in this publication was supported by the National Cancer Institute of the National Institutes of Health under Award Number R01CA222227. The content is solely the responsibility of the authors and does not necessarily represent the official views of the National Institutes of Health. We also acknowledge financial support from the University of North Carolina at Greensboro, the Natural Sciences and Engineering Council of Canada, the Canadian Institutes of Health Research, the Canadian Foundation for Innovation, the Nova Scotia Research and Innovation Trust, and Acadia University.

■ REFERENCES

(1) Juris, A.; Balzani, V.; Barigelletti, F.; Campagna, S.; Belser, P.; von Zelewsky, A. Ru(II) Polypyridine Complexes: Photophysics, Photochemistry, Eletrochemistry, and Chemiluminescence. *Coord. Chem. Rev.* **1988**, *84*, 85−277.
(2) Balzani, V.; Juris, A. Photochemistry and Photophysics of Ru(II) polypyridine Complexes in the Bologna Group. From Early Studies to Recent Developments. *Coord. Chem. Rev.* **2001**, *211*, 97−115.
(3) Campagna, S.; Puntoriero, F.; Nastasi, F.; Bergamini, G.; Balzani, V. Photochemistry and Photophysics of Coordination Compounds: Ruthenium. In *Photochemistry and Photophysics of Coordination Compounds I*; Balzani, V., Campagna, S., Eds.; Topics in Current Chemistry; Springer: Heidelberg, 2007; pp 117−214.
(4) Juris, A.; Campagna, S.; Balzani, V.; Gremaud, G.; Von Zelewsky, A. Absorption Spectra, Luminescence Properties, and Electrochemical Behavior of Tris-Heteroleptic Ruthenium(II) Polypyridine Complexes. *Inorg. Chem.* **1988**, *27*, 3652−3655.
(5) Knoll, J. D.; Turro, C. Control and Utilization of Ruthenium and Rhodium Metal Complex Excited States for Photoactivated Cancer Therapy. *Coord. Chem. Rev.* **2015**, *282*−*283*, 110−126.
(6) Mari, C.; Pierroz, V.; Ferrari, S.; Gasser, G. Combination of Ru(II) Complexes and Light: New Frontiers in Cancer Therapy. *Chem. Sci.* **2015**, *6*, 2660−2686.
(7) Glazer, E. C. Light-Activated Metal Complexes That Covalently Modify DNA. *Isr. J. Chem.* **2013**, *53*, 391−400.
(8) Zamora, A.; Denning, C. A.; Heidary, D. K.; Wachter, E.; Nease, L. A.; Ruiz, J.; Glazer, E. C. Ruthenium-Containing P450 Inhibitors for Dual Enzyme Inhibition and DNA Damage. *Dalton Trans.* **2017**, *46*, 2165−2173.
(9) Li, A.; Yadav, R.; White, J. K.; Herroon, M. K.; Callahan, B. P.; Podgorski, I.; Turro, C.; Scott, E. E.; Kodanko, J. J. Illuminating Cytochrome P450 Binding: Ru(II)-Caged Inhibitors of CYP17A1. *Chem. Commun.* **2017**, *53*, 3673−3676.
(10) Poynton, F. E.; Bright, S. A.; Blasco, S.; Williams, D. C.; Kelly, J. M.; Gunnlaugsson, T. The Development of Ruthenium(II) Polypyridyl Complexes and Conjugates for in Vitro Cellular and in Vivo Applications. *Chem. Soc. Rev.* **2017**, *46*, 7706−7756.
(11) White, J. K.; Schmehl, R. H.; Turro, C. An Overview of Photosubstitution Reactions of Ru(II) Imine Complexes and Their Application in Photobiology and Photodynamic Therapy. *Inorg. Chim. Acta* **2017**, *454*, 7−20.
(12) Ertl, C. D.; Ris, D. P.; Meier, S. C.; Constable, E. C.; Housecroft, C. E.; Neuburger, M.; Zampese, J. A. Sticking and Patching: Tuning and Anchoring Cyclometallated Ruthenium(II) Complexes. *Dalton Trans.* **2015**, *44*, 1557−1570.
(13) Allen, F. H. The Cambridge Structural Database: A Quarter of a Million Crystal Structures and Rising. *Acta Crystallogr., Sect. B: Struct. Sci.* **2002**, *58*, 380−388.
(14) Caspar, J. V.; Meyer, T. J. Application of the Energy Gap Law to Nonradiative, Excited-State Decay. *J. Phys. Chem.* **1983**, *87* (6), 952−957.
(15) Muro-Small, M. L.; Yarnell, J. E.; McCusker, C. E.; Castellano, F. N. Spectroscopy and Photophysics in Cyclometalated RuII−Bis(Bipyridyl) Complexes. *Eur. J. Inorg. Chem.* **2012**, *2012*, 4004−4011.
(16) Albani, B. A.; Peña, B.; Dunbar, K. R.; Turro, C. New Cyclometallated Ru(II) Complex for Potential Application in Photochemotherapy? *Photochem. Photobiol. Sci.* **2014**, *13*, 272−280.
(17) Sainuddin, T.; McCain, J.; Pinto, M.; Yin, H.; Gibson, J.; Hetu, M.; McFarland, S. A. Organometallic Ru(II) Photosensitizers Derived from ″-Expansive Cyclometalating Ligands: Surprising Theranostic PDT Effects. *Inorg. Chem.* **2016**, *55*, 83−95.
(18) Peña, B.; David, A.; Pavani, C.; Baptista, M. S.; Pellois, J.-P.; Turro, C.; Dunbar, K. R. Cytotoxicity Studies of Cyclometallated Ruthenium(II) Compounds: New Applications for Ruthenium Dyes. *Organometallics* **2014**, *33*, 1100−1103.
(19) Huang, H.; Zhang, P.; Chen, H.; Ji, L.; Chao, H. Comparison between Polypyridyl and Cyclometalated Ruthenium(II) Complexes: Anticancer Activities against 2D and 3D Cancer Models. *Chem. - Eur. J.* **2015**, *21*, 715−725.
(20) Shi, G.; Monro, S.; Hennigar, R.; Colpitts, J.; Fong, J.; Kasimova, K.; Yin, H.; DeCoste, R.; Spencer, C.; Chamberlain, L.; et al. Ru(II) Dyads Derived from Alpha-Oligothiophenes: A New Class of Potent and Versatile Photosensitizers for PDT. *Coord. Chem. Rev.* **2015**, *282*−*283*, 127−138.
(21) Sullivan, B. P.; Salmon, D. J.; Meyer, T. J. Mixed Phosphine 2,2′-Bipyridine Complexes of Ruthenium. *Inorg. Chem.* **1978**, *17*, 3334−3341.
(22) Fraval, J. T.; Godfrey, M. T. United States Patent. 2013, *1* (12), 5.
(23) Chen, R.; Yang, X.; Tian, H.; Wang, X.; Hagfeldt, A.; Sun, L. Effect of Tetrahydroquinoline Dyes Structure on the Performance of Organic Dye-Sensitized Solar Cells. *Chem. Mater.* **2007**, *19*, 4007−4015.
(24) Foxon, S. P.; Metcalfe, C.; Adams, H.; Webb, M.; Thomas, J. A. Electrochemical and Photophysical Properties of DNA Metallo-Intercalators Containing the Ruthenium(II) Tris(1-Pyrazolyl)Methane Unit. *Inorg. Chem.* **2007**, *46*, 409−416.
(25) Suzuki, K.; Kobayashi, A.; Kaneko, S.; Takehira, K.; Yoshihara, T.; Ishida, H.; Shiina, Y.; Oishi, S.; Tobita, S. Reevaluation of Absolute Luminescence Quantum Yields of Standard Solutions Using a Spectrometer with an Integrating Sphere and a Back-Thinned CCD Detector. *Phys. Chem. Chem. Phys.* **2009**, *11*, 9850−9860.
(26) DeRosa, M. C.; Crutchley, R. J. Photosensitized Singlet Oxygen and Its Applications. *Coord. Chem. Rev.* **2002**, *233-234*, 351−371.
(27) Bomben, P.; Robson, K.; Koivisto, B.; Berlinguette, C. Cyclometalated Ruthenium Chromophores for the Dye-Sensitized Solar Cell. *Coord. Chem. Rev.* **2012**, *256*, 1438−1450.
(28) Robson, K. C. D.; Koivisto, B. D.; Yella, A.; Sporinova, B.; Nazeeruddin, M. K.; Baumgartner, T.; Grätzel, M.; Berlinguette, C. P. Design and Development of Functionalized Cyclometalated Ruthenium Chromophores for Light-Harvesting Applications. *Inorg. Chem.* **2011**, *50*, 5494−5508.
(29) Bessho, T.; Yoneda, E.; Yum, J.-H.; Guglielmi, M.; Tavernelli, I.; Imai, H.; Rothlisberger, U.; Nazeeruddin, M. K.; Grätzel, M. New Paradigm in Molecular Engineering of Sensitizers for Solar Cell Applications. *J. Am. Chem. Soc.* **2009**, *131*, 5930−5934.
(30) Wang, L.; Yin, H.; Cui, P.; Hetu, M.; Wang, C.; Monro, S.; Schaller, R. D.; Cameron, C. G.; Liu, B.; Kilina, S.; et al. Near-Infrared-Emitting Heteroleptic Cationic Iridium Complexes Derived from 2,3-Diphenylbenzo[g]Quinoxaline as in Vitro Theranostic Photodynamic Therapy Agents. *Dalton Trans.* **2017**, *46*, 8091−8103.
(31) Koizumi, T. A.; Tomon, T.; Tanaka, K. Synthesis and Electrochemical Properties of Bis(Bipyridine)Ruthenium(II) Complexes Bearing Pyridinyl- and Pyridinylidene Ligands Induced by Cyclometalation of N′-Methylated Bipyridinium Analogs. *J. Organomet. Chem.* **2005**, *690*, 1258−1264.

DOI: 10.1021/acs.inorgchem.8b00689
Inorg. Chem. XXXX, XXX, XXX−XXX

(32) Gelens, E.; De Kanter, F. J. J.; Schmitz, R. F.; Sliedregt, L. A. J. M.; Van Steen, B. J.; Kruse, C. G.; Leurs, R.; Groen, M. B.; Orru, R. V. A. Efficient Library Synthesis of Imidazoles Using a Multicomponent Reaction and Microwave Irradiation. *Mol. Diversity* **2006**, *10*, 17−22.
(33) Braven, J.; Hanson, R. W.; Smith, N. G. Synthetic Routes to Indenopyridine Analogues of Morphactins. *J. Heterocycl. Chem.* **1995**, *32*, 1051−1055.
(34) Sasaki, I.; Vendier, L.; Sournia-Saquet, A.; Lacroix, P. G. Facile Synthesis of Cyclometalated Ruthenium Complexes with Substituted Phenylpyridines. *Eur. J. Inorg. Chem.* **2006**, *2006*, 3294−3302.
(35) Reveco, P.; Medley, J. H.; Garber, A. R.; Bhacca, N. S.; Selbin, J. Study of a Cyclometalated Complex of Ruthenium by 400-MHz Two-Dimensional Proton NMR. *Inorg. Chem.* **1985**, *24*, 1096−1099.
(36) Schatzschneider, U.; Niesel, J.; Ott, I.; Gust, R.; Alborzinia, H.; Wölfl, S. Cellular Uptake, Cytotoxicity, and Metabolic Profiling of Human Cancer Cells Treated with Ruthenium(II) Polypyridyl Complexes $[Ru(Bpy)_2(N^N)]Cl_2$ with N^N = bpy, phen, dpq, dppz, and dppn. *ChemMedChem* **2008**, *3*, 1104−1109.
(37) Fetzer, L.; Boff, B.; Ali, M.; Xiangjun, M.; Collin, J.-P.; Sirlin, C.; Gaiddon, C.; Pfeffer, M. Library of Second-Generation Cyclometalated Compounds and Evaluation of Their Biological Properties as Potential Anticancer Drugs: Passing the Nanomolar Barrier. *Dalton Trans.* **2011**, *40*, 8869−8878.
(38) Puckett, C. A.; Barton, J. K. Methods to Explore Cellular Uptake of Ruthenium Complexes. *J. Am. Chem. Soc.* **2007**, *129*, 46−47.
(39) Motley, T. C.; Troian-Gautier, L.; Brennaman, M. K.; Meyer, G. J. Excited-State Decay Pathways of Tris(Bidentate) Cyclometalated Ruthenium(II) Compounds. *Inorg. Chem.* **2017**, *56*, 13579−13592.
(40) Hissler, M.; Connick, W. B.; Geiger, D. K.; McGarrah, J. E.; Lipa, D.; Lachicotte, R. J.; Eisenberg, R. Platinum Diimine Bis(Acetylide) Complexes: Synthesis, Characterization, and Luminescence Properties. *Inorg. Chem.* **2000**, *39*, 447−457.
(41) McCusker, C. E.; McCusker, J. K. Synthesis and Spectroscopic Characterization of CN-Substituted Bipyridyl Complexes of Ru(II). *Inorg. Chem.* **2011**, *50*, 1656−1669.
(42) Kreitner, C.; Heinze, K. Excited State Decay of Cyclometalated Polypyridine Ruthenium Complexes: Insight from Theory and Experiment. *Dalton Trans.* **2016**, *45*, 13631−13647.
(43) McClenaghan, N. D.; Leydet, Y.; Maubert, B.; Indelli, M. T.; Campagna, S. Excited-State Equilibration: A Process Leading to Long-Lived Metal-to-Ligand Charge Transfer Luminescence in Supramolecular Systems. *Coord. Chem. Rev.* **2005**, *249*, 1336−1350.
(44) Majewski, M. B.; de Tacconi, N. R.; MacDonnell, F. M.; Wolf, M. O. Ligand-Triplet-Fueled Long-Lived Charge Separation in Ruthenium(II) Complexes with Bithienyl-Functionalized Ligands. *Inorg. Chem.* **2011**, *50*, 9939−9941.
(45) Barbieri, A.; Ventura, B.; Flamigni, L.; Barigelletti, F.; Fuhrmann, G.; Bäuerle, P.; Goeb, S.; Ziessel, R. Binuclear Wirelike Dimers Based on Ruthenium(II)−Bipyridine Units Linked by Ethynylene−Oligothiophene−Ethynylene Bridges. *Inorg. Chem.* **2005**, *44*, 8033−8043.
(46) Costa, R. D.; Aragó, J.; Ortí, E.; Pappenfus, T. M.; Mann, K. R.; Matczyszyn, K.; Samoc, M.; Zafra, J. L.; López Navarrete, J. T.; Casado, J. Impact of the Synergistic Collaboration of Oligothiophene Bridges and Ruthenium Complexes on the Optical Properties of Dumbbell-Shaped Compounds. *Chem. - Eur. J.* **2013**, *19*, 1476−1488.
(47) Liu, Y.; De Nicola, A.; Reiff, O.; Ziessel, R.; Schanze, K. S. Photophysics and Photoinduced Electron-Transfer Reactivity of Ruthenium(II) Complexes with Oligo(Thiophene-Bipyridine) Ligands,1. *J. Phys. Chem. A* **2003**, *107*, 3476−3485.
(48) Lincoln, R.; Kohler, L.; Monro, S.; Yin, H.; Stephenson, M.; Zong, R.; Chouai, A.; Dorsey, C.; Hennigar, R.; Thummel, R. P.; et al. Exploitation of Long-Lived 3IL Excited States for Metal−Organic Photodynamic Therapy: Verification in a Metastatic Melanoma Model. *J. Am. Chem. Soc.* **2013**, *135*, 17161−17175.
(49) Reichardt, C.; Pinto, M.; Wächtler, M.; Stephenson, M.; Kupfer, S.; Sainuddin, T.; Guthmuller, J.; McFarland, S. A.; Dietzek, B. Photophysics of Ru(II) Dyads Derived from Pyrenyl-Substitued Imidazo[4,5-f][1,10]Phenanthroline Ligands. *J. Phys. Chem. A* **2015**, *119*, 3986−3994.
(50) Sun, Y.; Joyce, L. E.; Dickson, N. M.; Turro, C. Efficient DNA Photocleavage by $[Ru(bpy)_2(dppn)]^{2+}$ with Visible Light. *Chem. Commun.* **2010**, *46*, 2426−2428.
(51) Wang, L.; Yin, H.; Jabed, M. A.; Hetu, M.; Wang, C.; Monro, S.; Zhu, X.; Kilina, S.; McFarland, S. A.; Sun, W. π-Expansive Heteroleptic Ruthenium(II) Complexes as Reverse Saturable Absorbers and Photosensitizers for Photodynamic Therapy. *Inorg. Chem.* **2017**, *56*, 3245−3259.
(52) de Melo, J. S.; Silva, L. M.; Arnaut, L. G.; Becker, R. S. Singlet and Triplet Energies of α-Oligothiophenes: A Spectroscopic, Theoretical, and Photoacoustic Study: Extrapolation to Polythiophene. *J. Chem. Phys.* **1999**, *111*, 5427−5433.
(53) Tyson, D. S.; Castellano, F. N. Intramolecular Singlet and Triplet Energy Transfer in a Ruthenium(II) Diimine Complex Containing Multiple Pyrenyl Chromophores. *J. Phys. Chem. A* **1999**, *103*, 10955−10960.
(54) Tyson, D. S.; Bialecki, J.; Castellano, F. N. Ruthenium(II) Complex with a Notably Longexcited State Lifetime. *Chem. Commun.* **2000**, 2355−2356.
(55) Tyson, D. S.; Henbest, K. B.; Bialecki, J.; Castellano, F. N. Excited State Processes in Ruthenium(II)/Pyrenyl Complexes Displaying Extended Lifetimes. *J. Phys. Chem. A* **2001**, *105*, 8154−8161.
(56) Tyson, D. S.; Luman, C. R.; Zhou, X.; Castellano, F. N. New Ru(II) Chromophores with Extended Excited-State Lifetimes. *Inorg. Chem.* **2001**, *40*, 4063−4071.
(57) Goze, C.; Kozlov, D. V.; Tyson, D. S.; Ziessel, R.; Castellano, F. N. Synthesis and Photophysics of Ruthenium(II) Complexes with Multiple Pyrenylethynylene Subunits. *New J. Chem.* **2003**, *27*, 1679−1683.
(58) Kozlov, D. V.; Tyson, D. S.; Goze, C.; Ziessel, R.; Castellano, F. N. Room Temperature Phosphorescence from Ruthenium(II) Complexes Bearing Conjugated Pyrenylethynylene Subunits. *Inorg. Chem.* **2004**, *43*, 6083−6092.
(59) Simon, J. A.; Curry, S. L.; Schmehl, R. H.; Schatz, T. R.; Piotrowiak, P.; Jin, X.; Thummel, R. P. Intramolecular Electronic Energy Transfer in Ruthenium(II) Diimine Donor/Pyrene Acceptor Complexes Linked by a Single C−C Bond. *J. Am. Chem. Soc.* **1997**, *119*, 11012−11022.
(60) Morales, A. F.; Accorsi, G.; Armaroli, N.; Barigelletti, F.; Pope, S. J. A.; Ward, M. D. Interplay of Light Antenna and Excitation "Energy Reservoir" Effects in a Bichromophoric System Based on Ruthenium−Polypyridine and Pyrene Units Linked by a Long and Flexible Poly(Ethylene Glycol) Chain†. *Inorg. Chem.* **2002**, *41*, 6711−6719.
(61) McClenaghan, N. D.; Barigelletti, F.; Maubert, B.; Campagna, S. Towards Ruthenium(II) Polypyridine Complexes with Prolonged and Predetermined Excited State Lifetimes. *Chem. Commun.* **2002**, 602−603.
(62) McCusker, J. K. Femtosecond Absorption Spectroscopy of Transition Metal Charge-Transfer Complexes. *Acc. Chem. Res.* **2003**, *36*, 876−887.
(63) Alberto, M. E.; Pirillo, J.; Russo, N.; Adamo, C. Theoretical Exploration of Type I/Type II Dual Photoreactivity of Promising Ru(II) Dyads for PDT Approach. *Inorg. Chem.* **2016**, *55*, 11185−11192.
(64) Majewski, M. B.; de Tacconi, N. R.; MacDonnell, F. M.; Wolf, M. O. Long-Lived, Directional Photoinduced Charge Separation in RuII Complexes Bearing Laminate Polypyridyl Ligands. *Chem. - Eur. J.* **2013**, *19*, 8331−8341.
(65) Moorlag, C.; Sarkar, B.; Sanrame, C. N.; Bäuerle, P.; Kaim, W.; Wolf, M. O. Conjugation Length Dependent Ground and Excited State Electronic Behavior in Oligothienyl Ru Complexes. *Inorg. Chem.* **2006**, *45*, 7044−7046.
(66) Monro, S.; Scott, J.; Chouai, A.; Lincoln, R.; Zong, R.; Thummel, R. P.; McFarland, S. A. Photobiological Activity of Ru(II)

DOI: 10.1021/acs.inorgchem.8b00689
Inorg. Chem. XXXX, XXX, XXX−XXX

Dyads Based on (Pyren-1-Yl)Ethynyl Derivatives of 1,10-Phenanthroline. *Inorg. Chem.* **2010**, *49*, 2889−2900.
(67) Croke, D. T.; Perrouault, L.; Sari, M. A.; Battioni, J.-P.; Mansuy, D.; Helene, C.; Le Doan, J. Structure-Activity Relationships for DNA Photocleavage by Cationic Porphyrins. *J. Photochem. Photobiol., B* **1993**, *18*, 41−50.
(68) Praseuth, D.; Gaudemer, A.; Verlhac, J.-B.; Kraljic, I.; Sissoëff, I.; Guillé, E. Photocleavage of Dna in the Presence of Synthetic Water-Soluble Porphyrins. *Photochem. Photobiol.* **1986**, *44*, 717−724.
(69) Armitage, B. A. *DNA Binders and Related Subjects*; Springer Science & Business Media, 2005.
(70) Puckett, C. A.; Barton, J. K. Mechanism of Cellular Uptake of a Ruthenium Polypyridyl Complex. *Biochemistry* **2008**, *47*, 11711−11716.
(71) Svensson, F. R.; Matson, M.; Li, M.; Lincoln, P. Lipophilic Ruthenium Complexes with Tuned Cell Membrane Affinity and Photoactivated Uptake. *Biophys. Chem.* **2010**, *149*, 102−106.

DOI: 10.1021/acs.inorgchem.8b00689
Inorg. Chem. XXXX, XXX, XXX−XXX